Manuscript Details

Manuscript number	HUMEV_2017_187_R2
Title	La Ferrassie 1: New perspectives on a “classic” Neandertal
Article type	Full Length Article

Abstract

The La Ferrassie 1 (LF1) skeleton, discovered over a century ago, is one of the most important Neandertal individuals both for its completeness and due to the role it has played historically in the interpretation of Neandertal anatomy and lifeways. Here we present new skeletal remains from this individual, which include a complete right middle ear ossicular chain (malleus, incus and stapes), three vertebral fragments and two costal remains. Additionally, the study of the skeleton has allowed us to identify new pathological lesions, including a congenital variant in the atlas, a greenstick fracture of the left clavicle and a lesion in a mid-thoracic rib of unknown etiology. In addition, we have quantified the amount of vertebral pathology, which is greater than previously appreciated. We have complemented the paleopathological analysis with a taphonomic analysis to identify any potential perimortem fractures. The taphonomic analysis indicates that no surface alteration is present in the LF1 skeleton and that the breakage pattern is that of bone which has lost collagen, which would be consistent with the intentional burial of this individual proposed by previous researchers. In this study we used CT and micro-CT scans in order to discover new skeletal elements, to better characterize the pathological lesions, and to quantify the fracture orientation of those bones in which the current plaster reconstruction did not allow its direct visualization, which underlines the broad potential of imaging technologies in paleoanthropological research. A century after its discovery, LF1 is still providing new insights into Neandertal anatomy and behavior.

Keywords	ear ossicles; vertebra; rib; paleopathology; taphonomy

Corresponding Author	Asier Gómez Olivencia
Order of Authors	Asier Gómez Olivencia, Rolf Quam, Nohemi Sala, Morgane Bardey Vaillant, James Ohman, antoine Balzeau

Submission Files Included in this PDF

File Name [File Type]

Answer to reviewers.doc [Response to Reviewers]

New fossils and Pathologies LF1-text-v.8.doc [Manuscript File]

Figure01.tif [Figure]

Figure02.tif [Figure]

Figure03.tif [Figure]

Figure04.tif [Figure]

Figure05.tif [Figure]

Figure06.tif [Figure]

Figure07.tif [Figure]

Figure08.tif [Figure]

Figure09.tif [Figure]

Tables-v.8.doc [Table]

Sup. Info-v.8.pdf [e-Component]

Submission Files Not Included in this PDF

File Name [File Type]

La Ferrassie 1 Right Incus.stl.zip [3D Models (.zip)]

La Ferrassie 1 Right Malleus.stl.zip [3D Models (.zip)]

La Ferrassie 1 Right Stapes.stl.zip [3D Models (.zip)]

To view all the submission files, including those not included in the PDF, click on the manuscript title on your EVISE Homepage, then click 'Download zip file'.

This manuscript contains content innovation file(s).
General instructions for reviewing content innovation files can be found here.

Dear Dr. Plavcan,
We have corrected the manuscript following the copy-editor's suggestion in most cases with only two exceptions:
1-we have left the number of the sections, as it is the current format in JHE
2-we have left “incudes” (and not incuses), following one of the reviewer's comments as it is the correct way to denominate the plural of incus.

Thank you.
Kind regards.
Asier Gómez-Olivencia

La Ferrassie 1: New perspectives on a "classic" Neandertal

Asier Gómez-Olivencia[a, b, c, d, *], Rolf Quam[e, f, d], Nohemi Sala[g, d], Morgane Bardey[c], James C. Ohman[h, i], Antoine Balzeau[c, j]

[a]Dept. Estratigrafía y Paleontología, Facultad de Ciencia y Tecnología, Euskal Herriko Unibertsitatea, UPV-EHU. Barrio Sarriena s/n, 48940 Leioa, Spain

[b]IKERBASQUE. Basque Foundation for Science, 48013 Bilbao, Spain

[c]Équipe de Paléontologie Humaine, UMR 7194, CNRS, Département Homme et Environnement, Muséum national d'Histoire naturelle. Musée de l'Homme, 17, Place du Trocadéro, 75016 Paris, France

[d]Centro UCM-ISCIII de Investigación sobre Evolución y Comportamiento Humanos, Avda. Monforte de Lemos 5 (Pabellón 14), 28029 Madrid, Spain

[e]Department of Anthropology, Binghamton University (SUNY), Binghamton, NY 13902, USA

[f]Division of Anthropology, American Museum of Natural History, Central Park West@79th St., New York, NY 10024, USA

[g]Grupo de Investigación en Bioacústica Evolutiva y Paleoantropología. Área de Antropología Física, Departamento de Ciencias de la Vida. Universidad de Alcalá, 28871 Alcalá de Henares, Madrid, Spain

[h]Research Centre in Evolutionary Anthropology and Palaeoecology. School of Natural Sciences and Psychology. Liverpool John Moores University, Liverpool L3 3AF, UK

[i]Department of Physical Anthropology. Cleveland Museum of Natural History. 1 Wade Oval Drive. Cleveland, Ohio 44106, USA

[j]Department of African Zoology, Royal Museum for Central Africa, Tervuren, Belgium

* Corresponding author.

E-mail address: asier.gomezo@ehu.eus (A. Gómez-Olivencia)

Keywords: Ear ossicles; Vertebra; Rib; Paleopathology; Taphonomy

Abstract

The La Ferrassie 1 (LF1) skeleton, discovered over a century ago, is one of the most important Neandertal individuals both for its completeness and due to the role it has played historically in the interpretation of Neandertal anatomy and lifeways. Here we present new skeletal remains from this individual, which include a complete right middle ear ossicular chain (malleus, incus, and stapes), three vertebral fragments, and two costal remains. Additionally, the study of the skeleton has allowed us to identify new pathological lesions, including a congenital variant in the atlas, a greenstick fracture of the left clavicle, and a lesion in a mid-thoracic rib of unknown etiology. In addition, we have quantified the amount of vertebral pathology, which is greater than previously appreciated. We have complemented the paleopathological analysis with a taphonomic analysis to identify any potential perimortem fractures. The taphonomic analysis indicates that no surface alteration is present in the LF1 skeleton and that the breakage pattern is that of bone that has lost collagen, which would be consistent with the intentional burial of this individual proposed by previous researchers. In this study, we used CT and microCT scans in order to discover new skeletal elements to better characterize the pathological lesions and to quantify the fracture orientation of those bones in which the current plaster reconstruction did not allow its direct visualization, which underlines the broad potential of imaging technologies in paleoanthropological research. A century after its discovery, LF1 is still providing new insights into Neandertal anatomy and behavior.

1. Introduction

New analytical and conceptual tools are providing the opportunity for paleoanthropologists to gain insights into fossil remains discovered a long time ago. Computed Tomography (CT) and microCT scans are providing new means to assess the fossil record, including the quantification of some anatomical features that were not previously (easily) accessible (e.g., Spoor et al., 1994; Stoessel et al., 2016a, b). These new technical means have also enlarged the available fossil record of certain bones that are not easily preserved, such as the ear ossicles (e.g., Gómez-Olivencia et al., 2015; Stoessel et al., 2016b), and have allowed researchers to develop novel approaches to studying the paleobiology of Pleistocene populations (Martínez et al, 2004, 2013; Quam et al, 2015).

At the same time, paleopathological and taphonomic approaches to hominin fossils represent complementary avenues of inquiry that, in combination, could be considered paleoforensic studies. These new approaches have already provided insights into important questions in human evolutionary studies. In particular, they are helping to clarify the anthropic origin of the Middle Pleistocene hominin accumulation at the site of the Sima de los Huesos (SH) in Spain (Arsuaga et al., 1990, 1997, 2014, 2015; Andrews and Fernández-Jalvo, 1997; Carbonell and Mosquera, 2006; Sala et al., 2014, 2015a, b, 2016). New excavations are providing evidence that complete human skeletons were accummulated in the SH (Arsuaga et al., 2014, 2015). Carnivores have been ruled out of the bone accummulation of the SH, as the carnivore activity on both bear and human bones at this site was subtle and performed by bears, which do not accummulate bones (Sala et al., 2014). Also, the SH human crania and long bones show

a post-mortem fracture pattern, compatible with collective burial assemblages (Sala et al., 2015a, b, 2016). Also, new taphonomic analyses have also given rise to an interesting debate about the accumulation of *Homo naledi* hominins at Dinaledi Chamber in South Africa (Dirks et al., 2015; Val, 2016). They are also providing new insights into the potential cause-of-death of iconic fossil specimens such as A.L. 288-1 "Lucy" (Kappelman et al., 2016). In these two cases, breakage analysis provided an additional tool in order to complement classical paleopathological analyses as it provides information on whether a bone was broken around the time of the death (perimortem) or after death (postmortem) once the collagen was lost (Sala et al., 2015a, b, 2016). In this context, in order to assess the breakage patterns, new imaging techniques based on CT-scans were used. The ongoing reassessment of the faunal collections from "classical" Neandertal sites (e.g., Spy, Regourdou, Goyet, Combe Grenal) has led to the identification of new fossil remains. Coupled with new dating and imaging technologies, as well as new taphonomic approaches, this is providing novel and important data on Neandertals (e.g., Crevecoeur et al., 2010; Gómez-Olivencia et al., 2013a, b; Maureille et al., 2015; Rougier et al., 2016). The recent reassessment of the faunal remains associated with the La Ferrassie 1 (LF1) Neandertal skeleton at the Musée de l'Homme (MH, Museum national d'Histoire naturelle, Paris) led to the identification of five new skeletal elements belonging to this individual. LF1 was found in 1909 and was removed from the site in at least two blocks of sediment (which also included stone tools and faunal remains) sealed in plaster and subsequently cleaned at the Musée de l'Homme by Marcellin Boule (Laville, 2007). The new fossils from LF1 correspond to three vertebral fragments and two costal remains that have not been

included in any previous studies.

This reassessment of the LF1 skeleton from an anatomical and taphonomic perspective also resulted in identifying previously undescribed bone anomalies in the axial and appendicular skeleton and provided the first taphonomic characterization of the LF1 skeleton. In addition, microCT scanning of the right temporal bone of LF1 led to the identification and virtual reconstruction of a complete ossicular chain (malleus, incus, and stapes) from the right side (Supplementary online material [SOM] .stl files; SOM Fig. S1).

The present study provides the first metric and morphological description of these new LF1 fossils, as well as comparison with other Pleistocene and recent humans. In addition, the bone anomalies are described and discussed in the context of previous pathologies documented for this same individual. A complete taphonomic analysis of the LF1 individual is also provided, with an emphasis on timing and causes of bone breakage that would complete the paleopathological assessment and might have implications for LF1's status as an intentional burial. These new results have implications for Neandertal anatomical variation and evolution, the paleobiology of the LF1 individual, and the taphonomic history of LF1 within the important archaeological sequence of the La Ferrassie rockshelter (Grand abri de la Ferrassie in French).

1.1. The La Ferrassie 1 skeleton

La Ferrassie rockshelter is located at the base of a limestone hill (Savignac de Miremont, Dordogne), five kilometers north of Le Bugue, France. This site preserves an important Middle and Upper Paleolithic sequence starting in MIS 5 (Turq et al., 2012;

Guérin et al., 2015; Frouin et al., 2017). On 17 September 1909, an adult male Neandertal skeleton, designated La Ferrassie 1 (LF1), was recovered from what Denis Peyrony considered a funeral pit contemporary to level C (Maureille and Van Peer, 1998). The following year, a second skeleton was found 50 cm west of LF1 (for a complete description of the history of the findings and the context see Heim [1976], Laville [2007], and references therein). This second skeleton belonged to an adult woman and was designated La Ferrassie 2 (LF2). These two skeletons were used as comparative (and complementary) specimens by Boule in his famous monograph on the La Chapelle-aux-Saints 1 specimen (Boule, 1911–13). The specimens LF1 and LF2 were later thoroughly described in a two-volume monograph (Heim, 1976, 1982b).

From 1912 to 1921, the remains of another four immature individuals were recovered from La Ferrassie: La Ferrassie 3, 4bis, 5, and 6 (Heim, 1982a). The right humerus and femur that were once labeled as La Ferrassie 4 actually belong to the Le Moustier 2 skeleton (Maureille, 2002), and thus LF4bis could now be named LF4. Finally, in 1970 and 1973, a fifth immature individual was found, La Ferrassie 8 (Heim, 1982a). Recent reassessment of the materials from the excavations by Delporte have yielded new remains from La Ferrassie 8 (Gómez-Olivencia et al., 2015) and several isolated dental remains that appear to represent additional adult individuals (Becam et al., 2015).

All the LF skeletons were intentionally buried according to Peyrony (1934) and Heim (1976). In fact, a report written by D. Peyrony in 1920 to the Ministère des Beaux-Arts explains that all five skeletons discovered until that moment show more or less the same orientation (East-West). The two adults (LF1 and LF2) had their heads

about 50 cm apart (Peyrony, 1934): LF2's head was located to the East and that of LF1 to the West. Moreover, the recent re-study of the archives from the different excavation periods show that LF1, LF2, and LF8, the three individuals for which more detailed information is available, had their head at a higher elevation than the rest of the body (Laville, 2007; Balzeau et al., 2016a, b). H. Breuil described LF1 as laying on an apparently natural depression (Maureille and Van Peer, 1998). D. Peyrony and M. Boule observed small packets of yellow sand (from the lower level) mixed with the Mousterian sediments associated with both LF1 and LF2, something not seen in the rest of the Mousterian levels. This has been interpreted as the effect of intentional funerary pits that removed sediment from the underlying level and mixed with that which afterwards filled the pit (Maureille and Van Peer, 1998). Both LF1 and LF2 are associated with the Ferrassie facies of the Mousterian. The geological levels they were discovered in are attributed to MIS3, between 54 ± 3 and 40 ± 2 ka (Guérin et al., 2015).

LF1 is a virtually complete skeleton that preserves all anatomical regions (Heim, 1976, 1982b; Fennell and Trinkaus, 1997; see SOM Table S1 and SOM Fig. S2). The bones missing in this skeleton are basically the patellae and small hand and foot bones. First, the presence of LF1 was recognized as a human femur and a human tibia were identified in the stratigraphic section. It is likely that one of the patellae was lost in the excavation that led to the unearthing of that stratigraphic section. The rest of the missing bones were either lost during the excavation process and/or were broken, which would have worsened their identifiability. It was determined to be male based on greater sciatic notch morphology of the pelvis (Heim, 1982b). The age-at-death of LF1 has been estimated to be between 40 and 55 years, and this individual has been classified as an

old adult (see Heim, 1976; Trinkaus, 1995). Our own assessment of the pubic symphysis is consistent with Todd's (1920) age phase X (50+; Meindl et al., 1985), which is consistent with previous estimations. Stature and body mass of this individual have been calculated at 171.0–173.1 cm and 85 kg (Ruff et al., 1997:their supplementary information; Carretero et al., 2012).

The pathological lesions present in LF1 include: alveolar mandibular abscesses related to a high degree of dental attrition; minor vertebral osteophytosis and osteoarthritis on one articular facet of a lumbar vertebra; presence of an exostosis that has reduced the size of the left transverse foramen of the atlas (C1); possible osteoarthritic changes of the right proximal radio-ulnar and left sacro-iliac articulation due to trauma; a healed fracture of the right femoral greater trochanter with abnormal bone growth in the trochanteric fossa (SOM Fig. S3); and bilateral periostitis on the distal femora and both proximal and distal ends of the tibiae (and presence on at least one fibula) as a result of a systemic condition, likely due to hypertrophic pulmonary osteoarthropathy (HPO) due to a thoracic infection and/or carcinoma (Dastugue, 1960; Heim, 1976, 1982b; Trinkaus, 1985; Fennell and Trinkaus, 1997). Regarding the femoral lesion, Dastugue (1960) described an osseous formation in the trochanteric fossa of the right femur. Trinkaus (1985:34) described the “abnormally enlarged” greater trochanter of the right femur as “the product of either an injury to the region affecting m. gluteus medius and/or m. obturator externus, or a fracture of the greater trochanter in which the detached portion was displaced proximomedially prior to healing.” In a subsequent study, Fennell and Trinkaus (1997) only mention the hypothesis of a healed fracture of the trochanter. Regarding the vertebral column,

Fennell and Trinkaus (1997:986) describe the presence of "minor vertebral osteophytosis and osteoarthritis of a lumbar facet," although Heim (1976:318) also noted that one lumbar vertebral body displays an osteophyte remarkable in size ("portent une exostose assez importante"). Gómez-Olivencia (2013) described in detail the vertebral remains of LF1, providing new anatomical determinations and detecting errors in the reconstruction of some of the vertebrae. He also provided a brief description of the pathological lesions present in the vertebrae, although he did not quantify them as Dawson and Trinkaus (1997) did with the spine of La Chapelle-aux-Saints 1.

2. Material and methods

The fossil remains of LF1 are housed at the Musée de l'Homme (MH, Museum national d'Histoire naturelle, Paris) and are available for study (requests should be made via http://colhelper.mnhn.fr/). The 3D models of the newly identified ossicles are available as SOM material to this article, which will allow further independent research on this material (Balzeau et al., 2010); the microCT from which they derive is also available (requests should be made using the previous link).

2.1. Ear ossicles

The anatomical description of the three ear ossicles refers to each of the bones within the tympanic cavity. In the case of the malleus, the tip of the manubrium is placed inferiorly, the manubrium itself laterally, the head medially and superiorly, and the articular facet posteriorly. In the case of the incus, the tip of the long process is

placed inferiorly and angled posteriorly, the short process placed superiorly and protruding posteriorly, the articular facet facing anteriorly, and the lowermost margin of the articular facet facing laterally to articulate with the malleus head. Finally, in the case of the stapes, the head is placed laterally to articulate with the tip of the incus long crus, the crura are located anteriorly and posteriorly, and the footplate is located medially with its long axis oriented anteroposteriorly.

The LF1 ear ossicles were compared with Pleistocene and recent hominin ossicles (SOM Table S2). Data from original fossil hominin specimens representing European Middle Pleistocene fossils, Neandertals, and Pleistocene *Homo sapiens* are included. Most data were collected by one of us (RQ) on original specimens, with additional data taken from the literature. Additional observations on early hominin ossicles representing *Australopithecus* and *Paranthropus* from southern Africa are discussed when relevant. The modern human sample consists of ossicles removed from cadavers during surgical dissection for gross anatomy instruction at the New York Chiropractic College in Seneca Falls, NY (USA; Quam, 2006).

Measurements of the ossicles follow previously outlined protocols (Quam et al., 2014) and consist of linear, angular, and area measurements of the individual bones (SOM Tables S3-S5). A recent study by Stoessel et al. (2016b) has provided additional data on a few measurements of Neandertal and fossil *H. sapiens* ear ossicles. Data have been included in the present study for the maximum length of the malleus, the long process length of the incus, and the height and footplate area of the stapes. Data for the lever arm (i.e., functional) lengths in the malleus and incus were also provided by Stoessel et al. (2016b), but were measured differently from the present study.

Nevertheless, the resultant lever ratio between the malleus and incus is similar to those in other studies and can be compared with the results presented here. We also provide some measurements for the LF8 stapes in addition to those that were published by Gómez-Olivencia et al. (2015).

The area of the stapes footplate can be estimated from the dimensions of the oval window when the stapes is not preserved. Prior studies have suggested that the footplate area can be estimated as 90% of the oval window area to account for the annular ligament (Martínez et al., 2004; Quam et al., 2013a; Stoessel et al., 2016b). This correction factor has been used for the oval window data published by Stoessel et al. (2016b) to provide a larger comparative context for LF1.

In addition to descriptive statistics for the comparative samples, statistical analysis included *t*-tests of a few variables that allowed for large enough sample sizes. In particular, significant differences between Neandertals and *H. sapiens* were examined for the malleus total length, incus long process length, and stapes total height and footplate area. Correlations between variables in the modern human sample (Quam et al., 2014) are also discussed where relevant for interpreting differences in the fossil specimens.

2.2. Paleopathological analysis

All postcranial elements of LF1 were examined macroscopically on multiple occasions. Radiographs and CT data (see below) were used to visualize the internal structure of those bones that showed external anomalies. The degenerative lesions present in the LF1 skeleton were quantified using a numerical code to describe the

presence and degree of development of the pathological lesions on the surfaces and edges of both vertebral bodies and articular facets (SOM Table S5), following Dawson and Trinkaus (1997) and Bridges (1994). The anatomical determination of the LF1 vertebrae followed Gómez-Olivencia (2013). To assess the potential presence of scoliosis, we measured the presence of asymmetry in the height of the vertebral body and in the articular pillars of the vertebrae and quantified the torsion and degree to which the spinous processes depart from the mid-sagittal plane defined from the vertebral body.

2.3. Taphonomic analysis

Surface analysis For the taphonomic analysis, 84 bone remains were studied, comprising all long and flat bones including the cranium. All bones were macroscopically and microscopically examined using a hand lens and a digital microscope (DINO-LITE™).

Breakage pattern The analysis of breakage patterns was focused on the long bones and cranial bones since these elements allows more accurate estimations for the timing and mechanisms of fracture (Sala et al., 2015a, 2016). This analysis followed different methodologies, depending on the skeletal element. For long bones, we followed the methodology proposed by Villa and Mahieu (1991) and Sala et al. (2015a) in terms of: fracture outline (longitudinal, transverse, or oblique/curved), fracture angle (right or oblique), fracture edge (smooth or jagged), shaft circumference (1: <50% of the circumference, 2: >50% of the circumference, 3: complete circumference), and shaft

fragment (1: <25% of the total diaphysis, 2: 25–50% of the total diaphysis, 3: 50–75% of the diaphysis, 4: >75% of the diaphysis). Previous studies have demonstrated that long bones with transverse fractures to the long axis, complete circumferences, and fracture edges with right angles and jagged surfaces are commonly associated with dry bone fractures (which occur postmortem), while oblique fractures with bevelled angles of the fracture plane, incomplete circumferences, and smooth surfaces are commonly associated with fresh or green bone fractures (perimortem; Villa and Mahieu, 1991; Sala et al., 2015a).

In the present study, our results are compared with bibliographic data and original observations made on different osteological assemblages, grouped by different taphonomic origins, in particular regarding the causes of the fracture. The long bone fracture pattern of LF1 was compared to two different groups. The first group is comprised of sites with assemblages considered standards of fresh bone fractures, such as in a cannibalism scenario: Fontbrégoua Neolithic site (data from Villa and Mahieu, 1991) or the Magdalenian assemblage from Brillenhöhle (data from Sala and Conard, 2016). The second comparative group consists of long bones from collective burials with evidence of breakage by sediment pressure: Late Neolithic collective burial of Sarrians site (Villa and Mahieu, 1991) and Sima de los Huesos hominins (Sala et al., 2015a).

For cranial remains, we followed the analytical method developed by Sala et al. (2016) in terms of: fracture outline (linear, depressed, stellate) ,fracture location, fracture angle (right or oblique), fracture edge (smooth or jagged), and presence/absence of cortical delamination. Fresh bone fractures can be identified by oblique angles,

smooth surfaces, the presence of cortical delamination, a pattern of depressed or stellate fracture outlines, and fractures crossing cranial sutures. In contrast, straight or linear fracture outline, right angles, jagged surfaces, absence of cortical delamination, and fractures interrupted by cranial sutures are more common in dry-bone or postmortem cranial fractures (Sala et al., 2016). For the cranial assemblages, we compared our results with bibliographic resources of osteological sites that are considered standards, in the literature, of fresh bone fractures (Agris Mesolithic site and Châteliers du Vieil-Auzay, France, from the Neolithic period) and dry bone fractures (the Neolithic site of Corconne and the Chalcolithic site of Villedubert, France; Jordana et al., 2013). Finally, the cranial breakage pattern of LF1 is also compared to original data on fossil specimens collected by one of us (NS), such as other adult Neandertal crania (La Chapelle-aux-Saints 1 and La Quina H5) and Sima de los Huesos cranial specimens (Sala et al., 2016).

Because both the cranial and postcranial remains of LF1 have been reconstructed using different glues and fillings (plaster/gypsum, wax; e.g., see Fennell and Trinkaus, 1997:their Figs. 3 and 4), the direct visualization of the fracture properties is occasionally obscured. For this reason, the fracture features were analyzed by using the CT scan images of long and cranial bones (SOM Fig. S4).

2.4. Radiographs and CT-scans

The clavicles of LF1 were radiographed using a Faxitron RX-650 (located at the MNHN) and were CT scanned in the Service de Radiologie Polyvalente, Hôpital de la Pitié-Salpètrière, Paris (pixel size = 0.35 mm, slice thickness = 0.5 mm). The CT scans

of the long bones and the cranium used for the taphonomic analysis range between 0.335 mm of slice thickness (and 0.259 mm of pixel size) for the femora to 0.131 mm of voxel size for the skull. One rib with an evident pathological lesion on its surface was microCT scanned using the AST-RX platform (UMS 2700, CNRS, and MNHN) with a voxel size of 0.056 mm. The LF1 temporal bones were also microCT scanned using the AST-RX platform (voxel size = 0.02365 mm). Multiplanar reformatting, thresholding procedures, three-dimensional volume rendering, and illustration acquisition were made with Avizo 6.1 (Mercury Computer Systems).

3. Description and comparison of new fossil remains from La Ferrassie 1 (LF1)

The careful assessment of the microCT scans has allowed us to virtually recover a complete chain of ear ossicles from the right temporal bone (the .stl models are added as SOM). No ear ossicles are preserved inside the left temporal bone. In addition, the revision of a box with indeterminate remains associated with LF1 has allowed us to identify five new human remains: three vertebral and two costal fragments.

3.1. Malleus

The LF1 malleus (Fig. 1, Table 1) is complete and well-preserved except for the missing tip of the lateral process. The position of this measurement point was estimated based on comparison with the complete manubrium in the LF3 malleus.

The manubrium in LF1 is curved with a flattened, spatulate tip and a well-developed and projecting lateral process. The head and neck join the manubrium

superiorly in a wide, open angle. A well-developed bony crest is present on the superior aspect of the neck and extends inferiorly onto the medial aspect. There is no gracile process and no tubercle for the tensor tympani muscle on the manubrium. There is no groove on the lateral aspect of the head, as described in the Qafzeh malleus (Arensburg and Nathan, 1972). However, there is a pronounced area of bone resorption on the anterior aspect of the head and neck. The articular facet is clearly delimited from the surrounding bone and covers most of the medial aspect of the head, with an inferior extension onto the inferior aspect of the head. The head is flattened in the ML direction, but shows a well-developed projection of bone on the superior aspect of the lateral face of the head.

The LF1 malleus compares favorably with the LF3 Neandertal malleus in all these anatomical details. The shape analysis performed by Stoessel et al. (2016b) shows that the Neandertal malleus differs from *H. sapiens* in showing, among other things, a relatively shorter manubrium and a more open angle between the manubrium and corpus. The manubrium length in the La Ferrassie Neandertals is nearly identical to the mean value in our recent *H. sapiens* sample, but LF1 shows longer length of the corpus (though not significantly), which would be consistent with the observation made by Stoessel et al. (2016b). Additionally, LF1 does show a wide angle between the manubrium and corpus, falling towards the upper end of the recent human range (see below).

The total length of the LF1 malleus (8.78 mm) is shorter than the Middle Pleistocene Ehringsdorf specimen, but nearly the same as in Biache 1 and falls within the Neandertal range of variation (Table 1). In contrast, fossil *H. sapiens* individuals

have uniformly shorter mallei, falling below the Neandertal range of variation, and the LF1 malleus is more than 1 s.d. above our recent human mean. A *t*-test reveals that Neandertals have significantly ($p = 0.033$) longer mallei than recent humans. The manubrium length in LF1 (4.90 mm) is nearly identical to that in the LF3 malleus, but both specimens show shorter manubria than the Middle Pleistocene AT-3746 specimen. The manubrium length is again uniformly shorter in fossil *H. sapiens*, but the recent human mean is very close to both the La Ferrassie specimens. The manubrium arc depth, reflecting the curvature of the manubrium, is similar in both the La Ferrassie mallei and deeper (i.e., more curved) than in fossil *H. sapiens* individuals. Nevertheless, higher values are found in our recent human sample.

The length of the corpus in LF1 (6.26 mm) is slightly shorter than in the Middle Pleistocene Biache 1 individual, but above the range of variation in fossil *H. sapiens* and longer than all but four individuals (c. 9%) in our recent human sample. The angle between the manubrium and the corpus (angle between the axes) in LF1 (140.6º) is similar to several fossil *H. sapiens* individuals and falls toward the upper end of the recent human range of variation. The width of the head in LF1 (2.60 mm) is smaller than in LF3 and the Middle Pleistocene Biache 1 individual (Table 1). Nevertheless, the head width does fall within the upper limit of the range of variation in fossil and recent *H. sapiens*.

3.2. Incus

The LF1 incus (Fig. 1, Table 2) is complete and well-preserved. The superior margin of the short process is slightly concave moving towards the rounded and bulbous

tip. A clear notch is present along the medial aspect of the inferior margin of the short process, close to the tip. The medial aspect of the incus body shows a deeply excavated depression. The long process is gently curved along its anterior margin, and the angle between the long and short processes is fairly closed (see below).

The LF1 incus compares favorably with both the LF3 and Amud 7 Neandertal incudes in most features. Like LF1, both of the latter show a concave superior border of the short process, a well-defined notch along the lower margin of the short process, as well as a bulbous short process tip. The presence of a notch in the incus short process is a well-known anatomical variant in *H. sapiens* (Arensburg and Nathan, 1971). The notch is located at the insertion point of the posterior incudal ligament, and its presence has been linked with this anatomical structure. All four incudes from the site of Qafzeh show the presence of a notch. Within our recent human sample, a notch occurs in 10.8% of individuals, and frequencies of this feature range from 30–100% in recent human populations (Mutaw, 1988). The shape of the short process tip is more variable in fossil and recent *H. sapiens*, ranging from bulbous to pointed. This range of variation is seen within the Qafzeh sample, with some specimens (Q11, Q12) showing a bulbous tip similar to that seen in the Neandertals and others (Q15, Q21) showing a more pointed tip.

Neandertal incudes are generally characterized by a straight long process (Heim, 1982a) as seen in the LF3, Amud 7, and Le Moustier 1 specimens (Ponce de León and Zollikofer, 1999; Quam et al., 2013a). The long process in LF1 is somewhat more curved than these other Neandertal individuals. The medial surface of the incus body in LF1 shows a well-excavated depression, giving a "wasted" aspect to the bone in this

region, and a similar depression is also seen on the medial aspect of the incus body in LF3 and Amud 7. While a shallow depression is also commonly seen on the medial body in recent humans, it is considerably more pronounced in the Neandertal specimens. Among the Qafzeh specimens, only Q15 approaches the degree of expression seen in the Neandertals, while the remaining three specimens show a considerably milder expression, more similar to recent humans.

The short process length in LF1 (5.26 mm) is clearly longer than the middle Pleistocene specimen Biache 1, as well as the LF3 and Amud 7 Neandertals (Table 2). The short process in LF1 also falls above the mean, but well within the ranges of variation, in fossil and recent humans. Similarly, Neandertals seem to have slightly shorter long processes than their middle Pleistocene ancestors. The long process length in LF1 (7.22 mm) is slightly longer than in either LF3 or Amud 7, but is nearly identical to the Neandertal mean reported by Stoessel et al. (2016b). The value in LF1 is above the upper limit of the range of variation seen in fossil *H. sapiens*, but is within the variation found in our recent human sample. Regarding the long processes, a *t*-test reveals that those of Neandertals are significantly ($p < 0.001$) longer than those of recent humans. Nevertheless, the resulting incudal index, comparing the long and short process lengths, is fairly similar in Neandertals and *H. sapiens*.

The arc depth (curvature) of the long process in LF1 (0.55 mm) is deeper (more curved) than in either LF3 or Amud 7 and is similar to the mean value in our recent human sample (Table 2). All of the Neandertal specimens fall towards the lower end of the range of variation in recent humans. The functional length in LF1 (4.25 mm) is slightly shorter than that reported for the middle Pleistocene Biache 1 individual, but

longer than LF3 or Amud 7. All of these specimens are close to or fall above the upper limit of variation in fossil *H. sapiens* specimens, and only Dolní Věstonice 14 overlaps with the Neandertal values. In contrast, the articular facet in the Neandertals is taller than in *H. sapiens*, with the values in both LF1 and Amud 7 falling above the upper limit of the fossil and recent *H. sapiens* ranges of variation.

The interprocess length in Neandertals, including LF1, is slightly shorter than in Biache 1, and all of the Neandertals fall toward the lower end of the fossil and recent *H. sapiens* ranges of variation (Table 2). The interprocess arc depth seems fairly similar in fossil and recent *H. sapiens*, but is deeper in LF1 and, particularly, Amud 7. The angle between the short and long processes is more closed in Neandertals than in fossil and recent *H. sapiens*, with little overlap in the range of values. The value in LF1 (53.7º) is closest to Qafzeh 11 (52.4º) among the *H. sapiens* samples. The more closed angle between the short and long processes in Neandertals is likely a primitive feature of their ossicles, since similarly low values have been reported in the early hominin *Paranthropus robustus* individual SKW 18 from South Africa, as well as in chimpanzees (Quam et al., 2013b).

3.3. Middle ear lever ratio

The functional lengths (i.e., lever arms) of the malleus and incus can be compared to one another to derive the middle ear lever ratio, an important physiological variable in modeling audition (Martínez et al., 2004, 2013). For the malleus, the functional length corresponds to the manubrium length, while for the incus it is measured from the rotational axis to the tip of the long process. Stoessel et al. (2016b)

have measured the functional lengths in the malleus and incus based on defining the center of mass of the ossicles. This corresponds approximately to the center of the articular facets. While the values for the individual malleus and incus lever arms reported by Stoessel et al. (2016b) are higher than those in the present study, the resultant lever ratio is comparable with the data in the present study since the mean lever ratio and the range of values are very similar between a sample of recent humans measured by Stoessel et al. (2016b) and us (Table 3). These values are also similar to those reported for modern humans in other studies (Dahmann, 1929, 1930; Rosowski, 1996).

The malleus and incus functional lengths in both LF1 and LF3 are slightly shorter than in the Middle Pleistocene individual from the Atapuerca Sima de los Huesos (SH) site (Table 3). Nevertheless, the lever ratios are quite similar in all three individuals. Indeed, there seems to be little difference in the lever ratio in any of the fossil or recent *Homo* samples in the present study. In contrast, chimpanzees show a higher lever ratio due to the combination of a long manubrium and short functional length, and the lever ratio in *P. robustus* is intermediate between chimpanzees and humans (Quam et al., 2013b). Thus, the presence of a human-like lever ratio in LF1 is a derived condition of the genus *Homo*, attributable to a lengthening of the incus functional length.

3.4. Stapes

The LF1 stapes (Fig. 1) is complete and well-preserved and shows an oval/kidney-shaped footplate. There is no tubercle for the insertion of the stapedius

muscle, but the stapedial head is clearly anteriorly skewed and located nearly in line with the anterior crus. The obturator foramen is bounded by a much longer and more curved posterior crus and shorter, straighter anterior crus.

The anteriorly skewed head and asymmetrical crura in the LF1 stapes are features that characterize Neandertals more generally. The asymmetrical crura are related to the anterior skew of the stapedial head, and these features were first described in the LF3 Neandertal (Heim, 1982a) and subsequently reported in the Subalyuk 2 and Le Moustier 2 Neandertals (Maureille et al., 2002; Quam et al., 2013a). This appears to be a derived condition in Neandertals (Stoessel et al., 2016b), since early hominin stapes show a stapedial head that is centrally placed atop more symmetrical crura (Quam et al., 2013b). This is the condition generally seen in modern humans as well. While an anteriorly skewed stapedial head and asymmetrical crura do also occur as a less frequent variant in modern humans, the expression of these traits is constant and more pronounced in Neandertals (Stoessel et al., 2016b).

The stapes height in LF1 (3.04 mm) is taller than in LF3, LF8, and Subalyuk 2 (Table 4). LF1 is close to the mean value for a small sample of Neandertal specimens (3.11 mm), but is smaller than fossil *H. sapiens* individuals and is nearly two standard deviations below the mean of our modern human sample (3.44 mm). A *t*-test reveals that Neandertals have significantly ($p < 0.001$) shorter stapes than recent humans. The obturator foramen is widest near the footplate, and the width is greater than the height in LF1. The resulting index is high (120), much higher than the other fossil specimens, and even above the upper limits of our modern human sample. The high value for this index in LF1 is primarily due to the width, rather than the height, of the foramen.

The posterior crus is considerably longer and more curved than the relatively short, straight anterior crus in LF1, contributing to an asymmetrical appearance of the bone and the anteriorly skewed head. The crural index in LF1 is low (77.8), but similar to other Neandertals. Fossil and recent *H. sapiens* show higher values for this index and generally have a more symmetrical appearance, with the head approximately centered above the crura. Compared with our modern human sample, it is obvious that the main difference in LF1 is the shortened anterior crus. The angle between the anterior and posterior crura (Angle A = 52.1º) in LF1 and all of the other fossil specimens fall within the range of variation in our modern human sample. In contrast, the angles between the footplate and the anterior crus (Angle B = 78.3º) and the posterior crus (Angle C = 49.6º) are higher and lower than the values in our modern human sample, falling outside the range of variation, but comparing more favorably with LF3 and LF8.

The footplate length (2.74 mm) and width (1.49 mm) in LF1 are larger than in the LF3 and LF8 stapes (Table 5). Compared with fossil and recent *H. sapiens*, the footplate in LF1 is considerably shorter, but the width is similar. The resultant index in LF1 (54.4) is similar to that in LF8 and close to the mean of a Neandertal sample based on the oval window. Fossil and recent *H. sapiens* show lower values for the index, mainly as a result of their longer footplates. A *t*-test reveals that Neandertals have significantly ($p < 0.001$) smaller stapes footplate areas than recent humans. Nevertheless, the area of the footplate in LF1 (3.39 mm^2) is larger than any other Neandertal measured to date (Table 4), including LF3, LF8, and other individuals from this same site whose footplate area is estimated from the oval window. The closest Neandertal individual to LF1 is Le Moustier 1 (3.30 mm^2; Stoessel et al., 2016b), and

the value in LF1 is exceeded by one Middle Pleistocene Sima de los Huesos (SH) individual. In contrast, the footplate size in LF1 is identical to the mean values in samples of fossil and recent *H. sapiens*.

3.5. Vertebral and costal remains

Three new vertebral and two new costal remains belonging to LF1 (Fig. 2) have been identified that add to those previously known (Heim, 1976; Gómez-Olivencia, 2013). These comprise two fragments of thoracic vertebrae and a fragmentary lumbar vertebral body. The two thoracic and the two costal fragments come from a bag containing faunal elements associated to the LF1 skeleton ("Ossements animaux provenent de la sépulture La Ferrassie I nº23645"). The lumbar vertebral fragment comes from a bag that was labeled as remains likely belonging to LF1 ("Ossements très vraisemblablement attribués au squelette de LA FERRASSIE 1").

Fragment of a thoracic vertebra This fragment (label: 23645 1953-25) represents a small fragment of the vertebral body and left pedicle of a thoracic vertebra (Fig. 2a1, a2). It preserves the upper left demifacet for the articulation with the rib, although it is partially eroded. It also shows erosion to the caudo-lateral edge of the vertebral body. The annular epiphysis is completely fused, indicating adult status. There are signs of osteophytosis on the edges of the vertebral body, which is consistent with the attribution of this fragment to La Ferrassie 1. The preserved measurements are 20.7 mm craniocaudally, 20.0 mm dorsoventrally, and 12.3 mm mediolateraly. Due to the incompleteness of this specimen, standard measurements are not possible. Based on the

vertebral bodies, Gómez-Olivencia (2013) proposed that at least 10 out of the 12 thoracic vertebrae were present in the LF1 skeleton. This new fragment represents a new specimen, and LF1 now preserves a minimum of 11 (out of 12) thoracic elements based on the vertebral body. Based on the preserved anatomy of the fragment, it likely represents a T5-T8 (Gómez-Olivencia, 2013).

Articular facet of a thoracic vertebra This is the upper right facet of a thoracic vertebra (no label). The preserved measurements are 16.6 mm cranio-caudally, 11.9 mm dorsoventrally, and 11.4 mm mediolateraly. The facet measures 8.7 mm craniocaudally and has an estimated mediolateral value of 12.0 mm. The preserved measurements of the pedicle are 11.0 mm (cranio-caudally) and 4.5 mm (thickness).

Vertebral body of a lumbar vertebra This is a fragmentary vertebral body (labels: "La Fer. I 23645 1953-25" in white ink on "1910 8" in red ink). This specimen likely represents the lowermost (fifth) lumbar vertebra. Preserved measurements are approximately 33.1 mm craniocaudally, 33.6 mm mediolaterally, and 30.7 mm dorsoventrally. The annular epiphysis is visible and completely fused, which is consistent with the adult age-at-death of LF1. The body cranio-caudal ventral diameter (height; M1; 33.1 mm) is larger than other Neandertal specimens and above the range of variation of a modern human comparative sample (Gómez-Olivencia et al., 2017), which would be consistent with LF1 being one of the tallest Neandertal individuals (Ruff et al., 1997).

Neck and fragment of the articular tubercle of a left rib This fragment (maximum preserved dimension: 29.5 mm) preserves the neck (cranio-caudal dimension: 11.9 mm; thickness: 5.4 mm) and part of the articular tubercle of the rib (Fig. 3a1, a2). Based on the preserved length of the neck and its cranio-caudal dimension, we tentatively assign this fragment to a mid-thoracic rib (between the 4th and the 7th): more cranial ribs would show smaller cranio-caudal dimensions of the neck, while caudal-most ribs would show shorter necks in the vertebro-sternal direction.

This aspect of the Neandertal anatomy is still largely unexplored due to its limited preservation in the fossil record (García-Martínez et al., 2017).

Shaft fragment of a rib This specimen preserves 20.1 mm of the shaft, with a preserved craniocaudal dimension of 12.5 mm and a thickness of 8.8 mm. In caudal view, it shows a well developed costal groove. Unfortunately, its limited preservation precludes its siding.

It was not possible to refit any of the new vertebral or costal fragments to the original LF1 collection.

4. Newly detected bone anomalies: preliminary description

The descriptions of the newly observed/revised pathological lesions are presented by anatomical region: first the postcranial axial skeleton (vertebral column and costal skeleton), second the upper limb, and finally the lower limb. No perimortem trauma was found in the analysis of the bone breakage.

4.1. Vertebral column

Anomaly on the atlas Heim (1976) noted the small size of the left transverse foramen of the atlas (C1; Fig. 4) that he attributed to the presence of an exostosis. In our view, there is no sign that indicates that abnormal bone growth reduced the size of the foramen. Rather, we consider that the small size of the transverse foramen is consistent with a case of unilateral persistent first intersegmental artery. In this variant, the vertebral artery enters the spinal canal of the C1 directly from the transverse process of the C2, without going through the transverse process of the C1, hence resulting in the small size of the transverse foramen. This is a common variant, appearing in 3.8% unilaterally and 0.8% bilaterally in a sample of 1013 individuals (Hong et al., 2008). It results in a deep groove on the inner aspect of the ipsilateral side of the posterior arch of the atlas and the abnormal transverse foramina are significantly smaller in size (Hong et al., 2008). The C1 of LF1 shows asymmetry in the posterior arch (Fig. 4d), which suggests the presence of the left vertebral artery inside the vertebral foramen, a further indication of this variant.

Additional lesions and anomalies of the spine SOM Tables S6 and S7 display the quantification of the osteoarthritic lesions on the spine, following the system by Dawson and Trinkaus (1997; based on Bridges, 1994). For a complete description of the pathological lesions of each vertebra see Gómez-Olivencia (2013). There is no sign of ossification at the insertion point (entheso-exostosis) of the anterior ligament (on the ventral surfaces of the vertebral bodies), nor of the ligamenta flava (cranial and caudal edges of the laminae). Compared to La Chapelle-aux-Saints 1, LF1 does not have

substantial degeneration in the lower cervical spine (Trinkaus, 1985; Gómez-Olivencia, 2013b). Nevertheless, the amount of vertebral pathology displayed in LF1 is greater than previously was reported by Fennell and Trinkaus (1997).

The LF1 individual shows different signs of asymmetries in the spine indicative of scoliosis in the vertebral bodies, articular pillars, and spinous processes (Fig. 5, SOM Tables S8). The latter include deviations from the mid-sagittal plane and rotations of the spinous process (Fig. 5c, d). Based on this evidence, we can detect two abnormal scoliotic curvatures in the vertebral column: one in the lower lumbar region and another in the cervical region.

Remodeling in the articular facets of L4, L5, and the sacrum are larger on the left side. Additionally, the close approximation between the L5 transverse process and the left sacral ala has formed a pseudoarthrosis (Fig. 5c, d). Together with the clockwise rotation of the spinous process, this evidence likely indicates a scoliotic curvature of the spine, with the concavity to the left (from the dorsal view). In our view, this scoliosis could have been compensatory to the pathology of the right femur. However, it cannot be ruled out that the compensation could be due to other causes, such as the asymmetry of either the length of the lower limbs and/or the pelvis. Unfortunately, the fragmentary nature of the pelvis and the reconstruction of the long bones prohibit further assessment.

In the cervical column, there is evidence of intense remodeling in the left articulation between C2 and C3. In fact, the left articular pillar of C3 is cranio-caudally smaller when compared to its right side counterpart. This suggests a cervical spine with a scoliotic concavity to the left. Remodeling on the right side of the uncinate process of the C3 is consistent with this hypothesis, as the rotation of the C2 relative to the C3

would have caused the remodeling of C3 on its right side. The cause of this lesion is not known, but could be related to the spinal lesions in the lumbar region and/or postural changes due to the lesion in the left clavicle (see below), among other possible causes.

4.2. Costal skeleton

We have detected a bone anomaly on the shaft fragment, just sternal to the posterior angle, of a rib from the left side, classified by Heim (1976) as a 6th or 7th rib. This specimen represents a refit of two fragments. This rib shaft fragment preserves a maximum straight length of ca. 103 mm, which starts close to the articular tubercle and includes the posterior angle. There are two abnormal bulges on the internal surface of the rib and a remodeled area on the external surface of the rib. The largest (ca. 16 mm × 3.5 mm) of these bulges (b1 in Fig. 6) is on the cranial edge of interior surface of the rib, while the second bulge (b2 in Fig. 6) is present on the caudal end of the internal surface of the rib near the internal edge of the costal groove. The first bulge (b1) is separated from the external surface by a shallow groove. The external surface of this rib, on the area affected by this bone anomaly, displays an area of ca. 29.5 mm in length by 15.5 mm in cranio-caudal direction that is more porous and may be due to bone remodeling. On this exterior surface, towards the cranial end of the rib, there are two abnormal ridges joining where a small fragment of bone protrudes from the surface (asterisk in Fig. 6). MicroCT analysis reveals that both bulges are likely expressions of a similar phenomenon. In section 1 (Fig. 1), it is possible to see the orientation of the original cortical bone beneath the largest bulge (b1). Two mutually non-exclusive hypotheses are posed to explain these anomalies: they could be related to a traumatic

event or they could be related to the hypertrophic pulmonary osteoarthropathy (Fennell and Trinkaus, 1997).

4.3. Upper limb: the left clavicle

Heim (1982b) provided a thorough metrical and morphological description of the clavicles of LF1. He suggested that the slightly (~1 mm) longer right clavicle was consistent with the hypothesis that this individual might have been left-handed (Heim, 1982b). He also recognized the strong asymmetry of the clavicles (Fig. 7) in frontal view, but did not provide an explanation for this asymmetry.

In cranial view, both clavicles look similar with the exception of a larger insertion for the M. deltoideus on the right clavicle. In dorsal view, the right clavicle is straight, while the lateral third of the left side clavicle is caudally oriented ca. 23º with respect to the medial half of the shaft (Fig. 7). Using the approach of Trinkaus et al. (1994) and Franciscus and Churchill (2002; i.e., absolute length difference divided by the smaller side times 100), the values provided by Voisin (2006) were used to calculate the asymmetry of the different curvatures of the clavicles of LF1. Neandertal individuals preserving both clavicles are rare, but surprisingly, despite the pathological lesion present on the left clavicle of LF1 (described below), this individual is not the Neandertal individual that displays the greatest percentage asymmetry (SOM Table S9). Regourdou 1 (R1; Vandermeersch and Trinkaus, 1995) shows a larger asymmetry in both the inferior and the superior curvatures in dorsal view (Voisin, 2006). The value of the inferior curvature could be affected by the fact that the acromial end of the left clavicle of R1 is broken. However, the value of the superior curvature would not be

affected by the missing fragment on the left clavicle and could be interpreted as asymmetry present in the upper limb of this individual due to his right-handedness (Volpato et al., 2012). Alternatively, the proposed methodology to measure the curvatures may not be suited to quantify the differences around the midshaft that we have detected in the LF1 individual.

On the left clavicle, at midshaft and again at about 65% distally, there are two "bumps" (see arrows in Fig. 9) with the shaft in between them slightly compressed cranio-caudally. A radiographic image of this section of the shaft is more "irregular," with regions of more dense trabeculae (SOM Fig. S5). At the equivalent location, the right clavicle displays a more organized trabecular orientation. This can also be seen in the CT-scans (Figs. 8–9), which also reveal differences in the shaft morphology.

We suggest that the morphological differences between the clavicles of LF1 are likely due to a well healed fracture of the left clavicle without bone displacement. The absence of a proper callus (except for the two "bumps") suggests this fracture likely occurred long before this individual's death, perhaps in childhood or early adulthood. Given the lack of evidence for a displaced fracture, it is probable this was a greenstick fracture in which the bone bends and partially breaks. There is one other example of a clavicular fracture in the Neandertal fossil record: clavicle Cl.8-149 from Krapina (Gardner and Smith, 2006) displays a healed fracture, but with bone displacement.

5. Taphonomic results

5.1. Bone surface

The LF1 skeleton is characterized by good preservation of bone surfaces. None of the analyzed LF1 remains shows any signs of hominin manipulation, such as cut-marks or intentional breakage. No evidence of carnivore activity, such as tooth marks, or small mammal activity, like rodent gnawing, was observed on the LF1 remains. Indeed, approximately 60% of the analyzed sample is intact bone remains in which no alterations of the bone surfaces or fractures are present. Regarding the post-depositional and/or postmortem modifications, no signs of trampling, carbonatic concretions or weathering, have been documented. Presence of manganese oxides was documented on 35.7% of the sample.

5.2. Fracture pattern

A total of 29 specimens (34.5% of the analyzed sample) display fractures, including the cranium, 21 long bone fragments, and seven other postcranial remains. The LF1 individual shows a fracture pattern characterized by the dominance of transverse fractures to the long axis, complete circumferences, and fracture edges with right angles (consistent with a preliminary assessment by Laville, 2007) and jagged surfaces (Table 6). Chi square values between the properties of long bone fractures of the LF1 sample and assemblages considered as showing typical postmortem fractures do not present significant differences regarding the fracture angle, fracture outline, or completeness of the circumference (Table 7). The same results are obtained when comparing the cranial fracture patterns with cranial samples interpreted as postmortem main fractures in terms of fracture angle or the presence of cortical delamination (Table 7). On the contrary, LF1 is significantly different in both the cranium and long bones

from those assemblages considered to show typical perimortem fractures for all the considered features (Table 7). This is consistent with a previous study, in which the LF1 cranium grouped with other Neandertal and Paleolithic *H. sapiens* specimens with typical postmortem features (Sala et al., 2016).

6. Discussion

The new results obtained in this study have important implications in terms of: a) broadening the known Neandertal variation for certain skeletal elements, such as the ear ossicles, and thus improving our general knowledge of the paleobiology of these extinct humans; b) providing new information regarding the paleobiology of the LF1 individual himself; and c) providing new evidence on the status of LF1 as an intentional burial.

6.1. Neandertal ear ossicle morphology and auditory implications

In his original study of the LF3 ossicular chain, the only one known at the time, Heim (1982a) suggested that Neandertals show some consistent differences from *H. sapiens*. Several of these observations have been confirmed by recent studies (Quam and Rak, 2008; Quam et al., 2013a; Stoessel et al., 2016b). Stoessel et al. (2016b) estimated the ancestral character state of the last common ancestor (LCA) of *Homo* and *Pan* and found Neandertals were more derived than recent *H. sapiens* in all three ossicles. Nevertheless, some of the features that distinguish the Neandertal ossicles from those of modern humans seem to be primitive retentions, since the Neandertals resemble the early hominins, while other features appear to be derived in the Neandertal ear

ossicles (Quam et al., 2013a, b; Stoessel et al., 2016b). Most of the features seen in Neandertal ossicles are also found among modern humans, and the Neandertal measurements are usually encompassed within the modern human range of variation. Although the sample size is small, Neandertal ossicles generally show a narrower range of morphological and metric variation than in modern humans.

The present study based on the ossicular chain of LF1 has confirmed that the Neandertal malleus is characterized by a similarly long but more curved manubrium, a larger head, and a more open angle between the manubrium and corpus when compared with modern humans. The incus of LF1 resembles other Neandertals in showing a longer and straighter long process, a more closed angle between the long and short processes, a larger articular facet, and a relatively "flattened" body. The present study agrees with previous suggestions for a slightly larger incudo-malleolar joint size in Neandertals (Quam et al., 2013a; Stoessel et al., 2016b). The Neandertals, including LF1, are derived in their longer incus functional length, and their lever ratio is similar to *H. sapiens*. However, the more closed angle between the long and short processes in Neandertals seems to reflect a primitive retention in their incus, with values similar to the early hominins and even chimpanzees (Quam et al., 2013b). A similar suite of features was also reported previously in the LF3 malleus and incus (Quam et al., 2013a).

Like other Neandertals, the LF1 stapes shows an asymmetrical configuration of the anterior and posterior crura and an anteriorly skewed stapedial head, and this appears to be a derived condition. While the LF1 footplate resembles other Neandertals in its shape, the overall size of the footplate is the largest yet reported among

Neandertals, being close to the mean in our recent *H. sapiens* sample. The size of the stapes footplate in Neandertals is variable, with the smallest specimens showing values as small as those in early hominins and chimpanzees, while larger specimens are similar in size to modern humans (Quam et al., 2013a). Values for the footplate area can be measured or estimated in five Neandertal individuals from La Ferrassie. The smallest individual, LF8, has a footplate area similar in size to some early hominin individuals, while LF1 represents the largest known Neandertal stapes. Only the Le Moustier 1 individual approximates the value found in LF1, and one of the Sima de los Huesos Middle Pleistocene individuals has a larger value.

The ossicular chain is the primary route for bony conduction of sound energy to the inner ear and has a central role in the hearing process (Wever and Lawrence, 1954). The proportions of the malleus and incus lever arms provide a mechanical advantage in transmitting the sound power from the outer ear to the cochlea, and the ratio between the sizes of the stapes footplate and tympanic membrane creates a pressure increase of the sound power reaching the inner ear (Rosowski, 2001). While much of the shape of the resultant audiogram is determined by the structures of the outer and middle ear, a recent study of Neandertal and modern human ear ossicles found a broad similarity in function, despite clear shape differences (Stoessel et al., 2016b). Specifically, the middle ear lever ratio and the stapes footplate/tympanic membrane area ratio were similar between these two groups. While these particular parameters can offer only limited insight into hearing abilities, the similarity between modern humans and Neandertals suggests their auditory capacities were also probably similar. The Sima de los Huesos Middle Pleistocene hominins, considered ancestors of the later Neandertals,

showed auditory capacities that were quite similar to those of modern humans (Martínez et al., 2004, 2013), while the early hominin taxa *Australopithecus* and *Paranthropus* showed auditory patterns that were distinct from modern humans (Quam et al., 2015).

6.2. Interrelationship, timing, and consequences of the different pathological lesions

In this study, evidence for the presence of additional anomalies and pathological lesions in LF1 are described. Altogether, LF1 displays an anomaly of the atlas (with no clinical consequences), clear signs of traumatic and degenerative lesions, as well as bilateral periostitis indicating a hypertrophic pulmonary osteoarthropathy due to a thoracic infection and/or carcinoma.

The anomaly of the atlas is the only congenital condition in LF1. The remaining various lesions occurred at different moments of this individual's life, but their onsets are difficult to establish. First, whether the two traumatic lesions (left clavicle and right femur) represent one or two events is currently unknown, but both clearly occurred long before death and most probably early in life. We hypothesize that the clavicular fracture was probably a greenstick fracture, while among the hypotheses posed to explain the fracture in the greater trochanter of the femur (Trinkaus, 1985), we prefer the avulsion fracture. It seems that LF1 displays a minimum of two scoliotic curvatures: one in the cervical region and one in the lower lumbar region. The degree of scoliosis of this individual was likely not very large. The scoliosis, at least in the lumbar region, could have resulted from the ongoing degenerative processes in the spine that occurred throughout adulthood. This process could have been aided by the possible postural asymmetry resulting from the femoral fracture. According to Fennell and Trinkaus

(1997), LF1 suffered from the early stages of an acute form of HPO, which likely began 2–14 months before death. Whether this HPO could be related to the lesion that we have detected in the rib is currently unknown.

Heim (1982b) suggested that the slightly (~1 mm) longer right clavicle was consistent with the hypothesis that this individual was left-handed. It is difficult to assess the extent to which the new pathology of the left clavicle contributed to its slightly shorter length, and thus Heim's assessment was biased by an undetected pathological lesion. The humeral asymmetry of LF1 demonstrated by Trinkaus et al. (1994) is strong evidence of a more robust right humerus, which suggests that LF1 was right-handed. The LF1 endocast also displays a morphological pattern of fronto-occipital petalia (i.e., a more anteriorly projecting right frontal pole, a larger development in antero-lateral orientation of the anterior curve of the right frontal lobe in superior view, and a more posteriorly projecting occipital pole as reflected by the 3D quantification of these anatomical traits) that is more consistent with the pattern in right-handed modern humans (Balzeau et al., 2012a, b).

The lesions of LF1 would have likely affected his posture and appearance. The traumatic lesion of the shoulder would have likely resulted in an asymmetrical external appearance of the shoulders. The presence of scoliosis and degeneration of the spine (based on the osteophytes) suggest that the trunk of LF1 was not straight, although its fragmentary status precludes an assessment to infer the degree of scoliosis in this individual. In addition, the HPO would have resulted in digital clubbing (Fennell and Trinkaus, 1997). In summary, it is likely that the trauma and degenerative lesions present in LF1 were also reflected in his external appearance, which would be consistent

with LF1 being an old man that suffered various healed lesions during his life and had ongoing problems due to respiratory issues. In fact, Fennell and Trinkaus (1995) proposed the HPO as the likely cause of death of LF1.

6.3. Is the taphonomic evidence consistent with LF1 being an intentional burial?

In Europe and Western Asia, starting in MIS 5 there is an increase in the preservation of partial-to-complete individual skeletons belonging to both Neandertals and modern humans in caves and rock-shelters. Paleolithic burials of hominin fossils are typically identified by relying on the combination of: the presence of a burial pit, in situ anatomical position of skeletal elements, the general completeness of the bones, and/or the presence of grave goods (Gargett, 1999; Riel-Salvatore and Clark, 2001; Duday, 2009). Surprisingly, taphonomic analysis of the hominin remains themselves has not figured prominently in the discussion surrounding Paleolithic burials, and taphonomic analyses of hominin fossils are still rare in the literature and limited mainly to those cases with evidence of cannibalism (e.g., Defleur, 1999; Fernández-Jalvo et al., 1999; Saladié et al., 2012; Rougier et al., 2016; Sala and Conard, 2016). In this study, we present for the first time the taphonomic analysis of the LF1 skeleton based on direct observations of bone alterations.

In addition to the paleopathological studies, the analysis of fracture patterns helps to elucidate the timing and causes of bone fractures. Wet state fractures occur while the bone is still surrounded by muscles, periosteum, skin, and other soft tissues and still has plastic properties. Fresh fracturing can be antemortem (before death) and/or perimortem (around the time of death), with the latter exhibiting no evidence of healing

(Ubelaker and Adams, 1995; Ortner, 2008; Wedel and Galloway, 2014; Sala et al., 2015a, 2016), while postmortem fractures occur after the individual's death, on defleshed bones (Sala et al. 2015a). The LF1 long bones exhibit a fracture pattern characterized by the dominance of transverse fractures to the long axis, complete circumferences, and fracture edges with right angles and jagged surfaces. These attributes are expected in post-depositional (i.e., postmortem) fracturing. Regarding the cranial breakage in LF1, all fractures display linear outlines, right angles, jagged surfaces, fractures interrupted by sutures, and the absence of cortical delamination, which are all indicative of dry bone fractures (Sala et al., 2016). Furthermore, the comparison of LF1 with other modern and fossil samples allow us to suggest that all the cranial and postcranial fractures of this individual occurred postmortem, probably due to the sediment pressure, after the loss of soft tissues and the main organic fraction (i.e., collagen) of bones. Wet bone has more energy when it absorbs stress than a dry bone, and, therefore, a dry bone needs much less energy to be fractured than a wet bone (Evans, 1957). LF1 was identified in the profile and, in order to recover it, it was necessary to excavate approximately 5 m of sediment that was lying on top of the skeleton in a surface area of 4 m^2 (Laville, 2007). The pressure of 5 m of sediment was likely responsible for most of the fractures and the fact that the cranium was crushed.

In addition to the fracture patterns, no signs of perimortem bone damage were documented, such as carnivore activity or traces of anthropic modifications of the bone surfaces. Lastly, the absence of any sign of weathering, trampling, or any other indication of postmortem modifications by bone exposure to the surface, together with the completeness and good preservation of the bones, and the fact that they were found

articulated (Heim, 1976; Laville, 2007), indicates that the internment of the LF1 individual occurred quickly and shortly after death. These observations are consistent with the observations made at the site by D. Peyrony, who in a letter written to M. Boule in 1926 said that sediment from the lower stratigraphic level was found mixed with that of the level containing the human remains, which would be consistent with the digging of a funeral pit for this individual (Maureille and Van Peer, 1998). The East-West orientation of at least five of the skeletons found at the site and the fact that LF1 and LF2 were located in the same orientation but facing opposite directions suggest that the orientation of the corpses may also have had an anthropogenic origin (Laville, 2007). While the presence of cryoturbation is well known at the La Ferrassie site, the fact that LF1 preserves a large part of the skeleton in anatomical connection indicates that this individual was likely not affected to a large degree by these processes. Laville (2007) proposed that other parts of the rock shelter, more to the east (the sector where LF8 was found), were likely more affected by these geological processes, which would be consistent with the scatter of the bones of these individuals, which still preserve anatomical coherence but likely not connection (Heim, 1982a; Balzeau et al., 2016a, b).

Excavation of a pit for the deposition of a very well preserved Neandertal skeleton is also present in the Bouffia Bonneval for La Chapelle-aux-Saints 1 (LC1; Rendu et al., 2014, 2016; but see Dibble et al., 2015). The preservation and completeness of the LC1 skeleton is similar to that of LF1.

In summary, the taphonomic analysis of the LF1 individual is consistent with the corpse being buried shortly after death, and thus not suffering any carnivore modifications or any other external weathering process. The bones lost collagen and

were fractured in situ due to the weight of the overlying sediments, but the anatomical connection between the bones was not affected. The taphonomic data for LF1 combined with information on the context of the discovery of other individuals at the site are consistent with an anthropogenic origin for the LF1 burial. Neandertals seem to show a fairly complex mortuary behavior, and different treatments of the dead have been described in the fossil record. There is a good evidence for cannibalistic practices among Neandertals in different parts of Western Europe: El Sidrón, Moula-Guercy, or Goyet (Defleur et al., 1999; Rosas et al., 2006; Rougier et al., 2016). It is also likely that some Neandertal groups (Pettitt, 2011) also purposefully buried their dead, i.e., that they practiced funerary behavior. This would be the case of individuals such as LF1, LF2, La Chapelle-aux-Saints 1, Amud 7, and Le Moustier 2, among others (Hovers et al., 2000; Maureille, 2002; Rendu et al., 2014, 2016; Balzeau et al., 2016a, b). Differences in preservation between individuals at the same site (e.g., Dederiyeh) also suggest the possibility of different kinds of interment (primary vs secondary; Akazawa and Muhesen, 2003). We are far from knowing the extent of variation in the mortuary behavior of Neandertals, and new findings of Neandertal remains at open air sites (e.g., Ein Qashish, Been et al., 2017) may complicate the picture further. In any case, the presence of intentional burial in Neandertals is strengthened by even earlier evidence, during the Middle Pleistocene, of intentional treatment of the dead in the Neandertal lineage (Arsuaga et al., 1997; Sala et al., 2015b).

7. Summary and conclusions

The LF1 skeleton, discovered over a century ago, is one of the most important

Neandertal individuals both for its completeness and due to the important role it has played historically in the interpretation of Neandertal anatomy and lifeways (Boule 1911–13). Nevertheless, after more than 100 years of study, this specimen continues to offer new insights into our understanding of the Neandertals.

New analytical and research tools have allowed us to:

1) Identify new fossil remains belonging to this skeleton, comprising the three ear ossicles from the right-side temporal bone, three vertebral remains, and two rib fragments. While the costal and vertebral remains are fragmentary, the ear ossicles are complete and help us to better understand the range of variation of this anatomical region in Neandertals.

2) Identify new pathological anomalies that make the pathological record of this individual more complete and yet also complicated. The skeletal remains of LF1 show the presence of two traumatic lesions: a possible greenstick fracture in the left clavicle with no displacement of the bone and a possible avulsion fracture of the greater trochanter of the right femur with a medial displacement of the trochanter. The spine shows signs of degenerative osteoarthritis and mild signs of scoliosis, which in the lumbar region could be caused by instability due to the aforementioned femoral fracture. Both femora and tibiae, and the fibula, radius, and first metatarsal from the right side show periostitis. This evidence for chronic, systemic infection could be due to a hypertrophic pulmonary osteoarthropathy (HPO) related to a pulmonary infection or carcinoma. One of the ribs shows a pathological anomaly of unknown etiology that could be either (or both) of traumatic origin and/or related to the HPO. Finally, LF1 also presents a non-clinical variant in the vertebral artery, called unilateral persistent first

intersegmental artery, which has no clinical consequences.

3) Confirm that no surface alterations are present on the bones in the LF1 skeleton and that the breakage pattern is that of bone that has lost collagen, which would be consistent with the intentional burial of this individual proposed by previous studies.

Finally, use of imaging technologies has allowed us to: 1) identify and virtually extract the ear ossicles that were inside the right temporal bone; 2) visualize the pathological lesions present in LF1 more clearly; and 3) quantify the fracture properties in those bones in which the reconstruction with plaster (or other materials) was obscuring them. Over a century after its discovery, the LF1 Neandertal is still revealing new insights into Neandertal anatomy and behavior.

Acknowledgments

We would like to thank the following individuals and institutions for their permission accessing the important materials under their care: P. Mennecier, A. Froment, and D. Grimaud-Hervé (MNHN, Paris). We are also indebted to A. Fort, L. Huet, V. Laborde, and M. García Sanz for curatorial and technical assistance. Thanks to the Service de Radiologie Polyvalente, CHU Pitié-Salpêtrière, Paris, France, for the CT-scans. Thanks to all the curators that have provided access to the collections under their care in order to amass our ear ossicle comparative sample. Thanks to the UMS 2700 (outils et méthodes de la systématique intégrative CNRS-MNHN) and AST-RX (plate-forme d'accès scientifique à la tomographie à rayons X du MNHN) for the microCT scans of one of the ribs. We are indebted to E. Trinkaus, C.O. Lovejoy, L. Puymerail, E.R. Warby, A. Rodríguez-Hidalgo, and our colleagues from MNHN, BBP, PAVE-

Cambridge, and UCM-ISCIII for stimulating discussions. AGO had a Marie Curie Intra-European Fellowship during a part of this work. This research has also received support from the Spanish Ministerio de Economía y Competitividad (project CGL2015-65387-C3-2-P-MINECO/FEDER), Research Group IT1044-16 from the Eusko Jaurlaritza-Gobierno Vasco, and Group PPG17/05 from the Universidad del País Vasco-Euskal Herriko Unibertsitatea. This research received support from the SYNTHESYS Project http://www.synthesys.info/ that is financed by European Community Research Infrastructure Action under the FP7 "Capacities" Program (FR- TAF-5135).

References

Akazawa, T., Muhesen, T., (Eds.), 2003. Neanderthal burials. Excavations of the Dederiyeh cave (Afrin, Syria). KW Publications Ltd., Auckland.

Andrews, P., Fernández-Jalvo, Y., 1997. Surface modifications of the Sima de los Huesos fossil humans. J. Hum. Evol. 33, 191–217.

Arensburg, B., Nathan, H., 1971. Observations on a notch in the short (superior or posterior) process of the incus. Acta Anat. 78, 84–90.

Arensburg, B., Nathan, H., 1972. A propos de deux osselets de l'oreille moyenne d'un néandertaloïde trouvés a Qafzeh (Israel). L'Anthropologie (Paris) 76, 301–308.

Arsuaga, J.L., Carretero, J.M., Gracia, A., Martínez, I., 1990. Taphonomical analysis of the human sample from the Sima de los Huesos Middle Pleistocene site (Atapuerca/Ibeas, Spain). Hum. Evol. 5, 505–513.

Arsuaga, J.L., Martínez, I., Gracia, A., Carretero, J.M., Lorenzo, C., García, N., Ortega, A.I., 1997. Sima de los Huesos (Sierra de Atapuerca, Spain). The site. J. Hum. Evol. 33, 109–127.

Arsuaga, J.L., Martínez, I., Arnold, L.J., Aranburu, A., Gracia-Téllez, A., Sharp, W.D., Quam, R.M., Falguères, C., Pantoja-Pérez, A., Bischoff, J., Poza-Rey, E., Parés, J.M., Carretero, J.M., Demuro, M., Lorenzo, C., Sala, N., Martinón-Torres, M., García, N., Alcázar de Velasco, A., Cuenca-Bescós, G., Gómez-Olivencia, A., Moreno, D., Pablos, A., Shen, C.-C., Rodríguez, L., Ortega, A.I., García, R., Bonmatí, A., Bermúdez de Castro, J.M., Carbonell, E., 2014. Neandertal roots: Cranial and chronological evidence from Sima de los Huesos. Science 344, 1358–

1363.

Arsuaga, J.L., Carretero, J.-M., Lorenzo, C., Gómez-Olivencia, A., Pablos, A., Rodríguez, L., García-González, R., Bonmatí, A., Quam, R.M., Pantoja-Pérez, A., Martínez, I., Aranburu, A., Gracia-Téllez, A., Poza-Rey, E., Sala, N., García, N., Alcázar de Velasco, A., Cuenca-Bescós, G., Bermúdez de Castro, J.M., Carbonell, E., 2015. Postcranial morphology of the middle Pleistocene humans from Sima de los Huesos, Spain. Proc. Natl. Acad. Sci. 112*,* 11524–11529.

Balzeau, A., Crevecoeur, I., Rougier, H., Froment, A., Gilissen, E., Grimaud-Hervé, D., Mennecier, P., Semal, P., 2010. Applications of imaging methodologies to paleoanthropology: beneficial results relating to the preservation, management and development of collections. C.R. Palevol 9*,* 265–275.

Balzeau, A., Gilissen, E., Grimaud-Hervé, D., 2012a. Shared pattern of endocranial shape asymmetries among great apes, anatomically modern humans, and fossil hominins. PLoS One 7*,* e29581.

Balzeau, A., Holloway, R., Grimaud-Hervé, D., 2012b. Variations and asymmetries in regional brain surface in the genus *Homo*. J. Hum. Evol. 62*,* 696–706.

Balzeau, A., Crevecoeur, I., Gómez-Olivencia, A., 2016a. Death is just the beginning: a grave offering, burial evidence and Neandertals at La Ferrassie. Bull. Mém. Soc. Anthropol. Paris 28*,* 7.

Balzeau, A., Aldeias, V., Bruxelles, L., Chiotti, L., Crevecoeur, I., Daujeard, C., Dibble, H., Goldberg, P., Gómez-Olivencia, A., Guérin, G., Madelaine, S., Sandgathe, D., Schwab, C., Talamo, S., Hublin, J.J., Turq, A., 2016b. New Data on the Context of the La Ferrassie 8 Neandertal child skeleton (Grand Abri of La Ferrassie,

Dordogne, France). PESHE 5, 40.

Becam, G., Gómez-Olivencia, A., Gómez-Robles, A., Souday, C., Arnaud, J., Frelat, M.A., Madelaine, S., Turq, A., Verna, C., Balzeau, A., 2015. Restes dentaires isolés de La Ferrassie : nouveaux fossiles, révision des anciennes collections et implications. Bull. Mém. Soc. Anthropol. Paris 27, S11.

Been, E., Hovers, E., Ekshtain, R., Malinski-Buller, A., Agha, N., Barash, A., Mayer, D.E.B.-Y., Benazzi, S., Hublin, J.-J., Levin, L., Greenbaum, N., Mitki, N., Oxilia, G., Porat, N., Roskin, J., Soudack, M., Yeshurun, R., Shahack-Gross, R., Nir, N., Stahlschmidt, M.C., Rak, Y., Barzilai, O., 2017. The first Neanderthal remains from an open-air Middle Palaeolithic site in the Levant. Sci. Rep. 7, 2958.

Boule, M., 1911-1913. L'homme fossile de la Chapelle aux Saints. Ann. de Paléontol. 6:111–172; 7:21–56, 85–192; 8: 1–70.

Bridges, P.S., 1994. Vertebral arthritis and physical activities in the prehistoric Southeastern United States. Am. J. Phys. Anthropol. 93, 83–93.

Carbonell, E., Mosquera, M., 2006. The emergence of a symbolic behaviour: the sepulchral pit of Sima de los Huesos, Sierra de Atapuerca, Burgos, Spain. C.R. Palevol. 5, 155–160.

Carretero, J.M., Rodríguez, L., García-González, R., Arsuaga, J.L., Gómez-Olivencia, A., Lorenzo, C., Bonmatí, A., Gracia, A., Martínez, I., Quam, R., 2012. Stature estimation from complete long bones in the Middle Pleistocene humans from the Sima de los Huesos, Sierra de Atapuerca (Spain). J. Hum. Evol. 62, 242–255.

Crevecoeur, I., 2007. New discovery of an Upper Paleolithic auditory ossicle: The right malleus of Nazlet Khater 2. J. Hum. Evol. 52, 341–345.

Crevecoeur, I., Bayle, P., Rougier, H., Maureille, B., Higham, T., van der Plicht, J., De Clerck, N., Semal, P., 2010. The Spy VI child: A newly discovered Neandertal infant. J. Hum. Evol. 59, 641–656.

Dahmann, H., 1929. Zur physiologie der hörens; experimentelle untersuchungen über die mechanik der Gehörknöchelchenkette, sowie über deren verhalten auf ton und luftdruck. Z. Hals-Nasen-Ohrenheilk 24, 462–497.

Dahmann, H., 1930. Zur physiologie der hörens; experimentelle untersuchungen über die mechanik der Gehörknöchelchenkette, sowie über deren verhalten auf ton und luftdruck. Z. Hals-Nasen-Ohrenheilk 27, 329–368.

Dastugue, J., 1960. Pathologie de quelques Néandertaliens. Congrès des Sci. Anthropol. Et Ethnol. 1, 577–581.

Dawson, J.E., Trinkaus, E., 1997. Vertebral osteoarthritis of the La Chapelle-aux-Saints 1 Neanderthal. J. Archaeol. Sci. 24, 1015–1021.

Defleur, A., White, T.D., Valensi, P., Slimak, L., Crégut-Bonnoure, É., 1999. Neanderthal Cannibalism at Moula-Guercy, Ardéche, France. Science. 286, 128–131.

Dibble, H.L., Aldeias, V., Goldberg, P., McPherron, S.P., Sandgathe, D., Steele, T.E., 2015. A critical look at evidence from La Chapelle-aux-Saints supporting an intentional Neandertal burial. J. Archaeol. Sci. 53, 649–657.

Dirks, P.H., Berger, L. R., Roberts, E.M., Kramers, J.D., Hawks, J., Randolph-Quinney, P.S., Elliott, M., Musiba, C.M., Churchill, S.E., de Ruiter, D.J., Schmid, P., Backwell, L.R., Belyanin, G.A., Boshoff, P., Hunter, K.L., Feuerriegel, E.M., Gurtov, A., Harrison, J.d.G., Hunter, R., Kruger, A., Morris, H., Makhubela, T.

V., Peixotto, B., Tucker, S., 2015. Geological and taphonomic context for the new hominin species *Homo naledi* from the Dinaledi Chamber, South Africa. eLife 4, e09561.

Duday, H., 2009. The archaeology of the dead: Lectures in Archaeothanatology. Oxbow Books, Oxford.

Evans, F.G., 1957. Stress and Strain in Bones. Their Relation to Fractures and Osteogenesis. Charles C. Thomas, Springfield.

Fennell, K.J., Trinkaus, E., 1997. Bilateral femoral and tibial periostitis in the La Ferrassie 1 Neanderthal. J. Archaeol. Sci. 24, 985–995.

Fernández-Jalvo, Y., Díez, J.C., Cáceres, I., Rosell, J., 1999. Human cannibalism in the Early Pleistocene of Europe (Gran Dolina, Sierra de Atapuerca, Burgos, Spain). J. Hum. Evol. 37, 591–622.

Franciscus, R.G., Churchill, S.E., 2002. The costal skeleton of Shanidar 3 and a reappraisal of Neandertal thoracic morphology. J. Hum. Evol. 42, 303–356.

Frouin, M., Guérin, G., Lahaye, C., Mercier, N., Huot, S., Aldeias, V., Bruxelles, L., Chiotti, L., Dibble, H.L., Goldberg, P., Madelaine, S., McPherron, S.J.P., Sandgathe, D., Steele, T.E., Turq, A., 2017. New luminescence dating results based on polymineral fine grains from the Middle and Upper Palaeolithic site of La Ferrassie (Dordogne, SW France). Quatern. Geochronol. 39, 131–141.

García-Martínez, D., Bastir, M., Huguet, R., Estalrrich, A., García-Tabernero, A., Ríos, L., Cunha, E., de la Rasilla, M., Rosas, A., 2017. The costal remains of the El Sidrón Neanderthal site (Asturias, northern Spain) and their importance for understanding Neanderthal thorax morphology. J. Hum. Evol. 111, 85–101.

Gardner, J.C., Smith, F.H., 2006. The paleopathology of the Krapina Neandertals. Period. Biol. 108, 471–484.

Gargett, R.H., 1999. Middle Palaeolithic burial is not a dead issue: the view from Qafzeh, Saint-Cesaire, Kebara, Amud, and Dederiyeh. J. Hum. Evol. 37, 27–90.

Gómez-Olivencia, A., 2013. The presacral spine of the La Ferrassie 1 Neandertal: a revised inventory. Bull. Mém. Soc. Anthropol. Paris 25, 19–38.

Gómez-Olivencia, A., Couture-Veschambre, C., Madelaine, S., Maureille, B., 2013a. The vertebral column of the Regourdou 1 Neandertal. J. Hum. Evol. 64, 582–607.

Gómez-Olivencia, A., Garralda, M.D., Vandermeersch, B., Madelaine, S., Arsuaga, J.L., Maureille, B., 2013b. Two newly identified Mousterian human rib fragments from Combe-Grenal (Domme, France). Paleo 24, 229–234.

Gómez-Olivencia, A., Crevecoeur, I., Balzeau, A., 2015. La Ferrassie 8 Neandertal child reloaded: New remains and re-assessment of the original collection. J. Hum. Evol. 82, 107–126.

Gómez-Olivencia, A., Arlegi, M., Barash, A., Stock, J.T., Been, E., 2017. The Neandertal vertebral column 2: The lumbar spine. J. Hum. Evol. 106, 84–101.

Guérin, G., Frouin, M., Talamo, S., Aldeias, V., Bruxelles, L., Chiotti, L., Dibble, H.L., Goldberg, P., Hublin, J.-J., Jain, M., Lahaye, C., Madelaine, S., Maureille, B., McPherron, S.J.P., Mercier, N., Murray, A.S., Sandgathe, D., Steele, T.E., Thomsen, K.J., Turq, A., 2015. A multi-method luminescence dating of the Palaeolithic sequence of La Ferrassie based on new excavations adjacent to the La Ferrassie 1 and 2 skeletons. J. Archaeol. Sci. 58, 147–166.

Heim, J.-L., 1976. Les Hommes fossiles de la Ferrassie. I. Le gisement. Les squelettes

adultes (crâne et squelette du tronc). Masson, Paris.

Heim, J.-L., 1982a. Les enfants néandertaliens de la Ferrassie. Étude anthropologique et analyse ontogénique des hommes de Néandertal. Masson, Paris.

Heim, J.-L., 1982b. Les hommes fossiles de La Ferrassie. II. Les squelettes d'adultes: squelettes des membres. Masson, Paris.

Hong, J.T., Lee, S.W., Son, B.C., Sung, J.H., Yang, S.H., Kim, I.S., Park, C.K., 2008. Analysis of anatomical variations of bone and vascular structures around the posterior atlantal arch using three-dimensional computed tomography angiography. J. Neurosurg. Spine 8, 230–236.

Hovers, E., Kimbel, W.H., Rak, Y., 2000. The Amud 7 skeleton-still a burial. Response to Gargett. J. Hum. Evol. 39, 253–260.

Jordana, F., Colat-Parros, J., Bénézech, M., 2013. Breakage patterns in human cranial bones. Romanian J. Legal Med. 21, 287–292.

Kappelman, J., Ketcham, R.A., Pearce, S., Todd, L., Akins, W., Colbert, M.W., Feseha, M., Maisano, J.A., Witzel, A., 2016. Perimortem fractures in Lucy suggest mortality from fall out of tall tree. Nature 537, 503–507.

Laville, D., 2007. La Ferrassie : taphonomie d'un site sépulcral moustérien, Université de Liège

Lisoněk, P., Trinkaus, E., 2006. The auditory ossicles. In: Trinkaus, E., Svoboda, J. (Eds.), Early Modern Human Evolution in Central Europe: The People of Dolní Věstonice and Pavlov. Oxford University Press, Oxford, pp. 153–155.

Martínez, I., Arsuaga, J.-L., Quam, R., Lorenzo, C., Gracia, A., Carretero, J.-M., Rosa, M., Jarabo, P., Carbonell, E., Bermúdez De Castro, J.-M., 2004. Auditory

capacities in Middle Pleistocene humans from the Sierra de Atapuerca in Spain. Proc. Natl. Acad. Sci. 101, 9976–9981.

Martínez, I., Rosa, M., Quam, R., Jarabo, P., Lorenzo, C., Bonmatí, A., Gómez-Olivencia, A., Gracia, A., Arsuaga, J.L., 2013. Communicative capacities in Middle Pleistocene humans from the Sierra de Atapuerca in Spain. Quatern. Intl. 295, 94–101.

Maureille, B., 2002. A lost Neanderthal neonate found. Nature 419, 33–34.

Maureille, B., Van Peer, P., 1998. Une donnée peu connue sur la sépulture du premier adulte de La Ferrassie (Savignac-de-Miremont, Dordogne)/A little known element concerning the burial of the first adult at La Ferrassie (Savignac-de-Miremont, Dordogne). Paleo 10, 291–301.

Maureille, B., Gómez-Olivencia, A., Couture-Veschambre, C., Madelaine, S., Holliday, T., 2015. Nouveaux restes humains provenant du gisement de Regourdou (Montignac-sur-Vézère, Dordogne, France). Paleo 26, 117–138.

Meindl, R.S., Lovejoy, C.O., Mensforth, R.P., Walker, R.A., 1985. A revised method of age determination using the *os pubis*, with a review and tests of accuracy of other current methods of pubic symphyseal aging. Am. J. Phys. Anthropol. 68, 29–45.

Mutaw, R., 1988. Variation in the frequency of a notch in the short process of the incus in six different human skeletal populations. Intl. J. Anthropol. 3, 199–205.

Ortner, D., 2008. Differential diagnosis of skeletal injuries. In: Kimmerle, E.H., Baraybar, J.P. (Eds.), Skeletal trauma: identification of injuries resulting from human rights abuse and armed conflict. CRC Press, Boca Raton, pp. 21–86.

Pettitt, P.B., 2011. The Paleolithic origins of human burial. Routledge, London.

Peyrony, D., 1934. La Ferrassie. Moustérien, Périgordien, Aurignacien. Préhistoire III, 1–92.

Ponce de León, M., Zollikofer, C.P.E., 2013. The internal cranial morphology of Oase 2. In: Trinkaus, E., Constantin, S., Zilhão, J. (Eds.), Life and Death at the Pestera cu Oase. A Setting for Modern Human Emergence in Europe. Oxford University Press, Oxford, pp. 332–347.

Ponce De León, M.S., Zollikofer, C.P.E., 1999. New evidence from Le Moustier 1: Computer-assisted reconstruction and morphometry of the skull. Anat. Rec. 254, 474–489.

Quam, R., 2006. Temporal bone anatomy and the evolution of acoustic capacities in fossil humans. Ph.D. Dissertation, Binghamton University, SUNY

Quam, R., Rak, Y., 2008. Auditory ossicles from southwest Asian Mousterian sites. J. Hum. Evol. 54, 414–433.

Quam, R., Martínez, I., Arsuaga, J.L., 2013b. Reassessment of the La Ferrassie 3 Neandertal ossicular chain. J. Hum. Evol. 64, 250–262.

Quam, R., Martínez, I., Rosa, M., Bonmatí, A., Lorenzo, C., de Ruiter, D.J., Moggi-Cecchi, J., Conde Valverde, M., Jarabo, P., Menter, C.G., Thackeray, J.F., Arsuaga, J.L., 2015. Early hominin auditory capacities. Sci. Adv. 1(8), e1500355.

Quam, R.M., de Ruiter, D.J., Masali, M., Arsuaga, J.-L., Martínez, I., Moggi-Cecchi, J., 2013a. Early hominin auditory ossicles from South Africa. Proc. Natl. Acad. Sci. 110, 8847–8851.

Quam, R.M., Coleman, M.N., Martínez, I., 2014. Evolution of the auditory ossicles in extant hominids: metric variation in African apes and humans. J. Anat. 225, 167–

196.

Rendu, W., Beauval, C., Crevecoeur, I., Bayle, P., Balzeau, A., Bismuth, T., Bourguignon, L., Delfour, G., Faivre, J.-P., Lacrampe-Cuyaubère, F., Tavormina, C., Todisco, D., Turq, A., Maureille, B., 2014. Evidence supporting an intentional Neandertal burial at La Chapelle-aux-Saints. Proc. Natl. Acad. Sci. 111, 81–86.

Rendu, W., Beauval, C., Crevecoeur, I., Bayle, P., Balzeau, A., Bismuth, T., Bourguignon, L., Delfour, G., Faivre, J.-P., Lacrampe-Cuyaubère, F., Muth, X., Pasty, S., Semal, P., Tavormina, C., Todisco, D., Turq, A., Maureille, B., 2016. Let the dead speak…comments on Dibble et al.'s reply to "Evidence supporting an intentional burial at La Chapelle-aux-Saints". J. Archaeol. Sci. 69, 12–20.

Rosas, A., Martinez-Maza, C., Bastir, M., Garcia-Tabernero, A., Lalueza-Fox, C., Huguet, R., Ortiz, J.E., Julia, R., Soler, V., de Torres, T., Martinez, E., Canaveras, J.C., Sanchez-Moral, S., Cuezva, S., Lario, J., Santamaria, D., de la Rasilla, M., Fortea, J., 2006. Paleobiology and comparative morphology of a late Neandertal sample from El Sidrón, Asturias, Spain. Proc. Natl. Acad. Sci. 103, 19266–19271.

Rosowski, J., 1996. Models of external- and middle-ear function. In: Hawkins, H., McMullen, T., Popper, A., Fay, R. (Eds.), Auditory Computation. Springer, New York, pp. 15–61.

Rosowski, J., 2001. Introduction to the analysis of middle-ear function. In: Jahn, A., Santos-Sacchi (Eds.), Physiology of the Ear. Second Edition. Singular, San Diego, pp. 161–190.

Rougier, H., Crevecoeur, I., Beauval, C., Posth, C., Flas, D., Wißing, C., Furtwängler, A., Germonpré, M., Gómez-Olivencia, A., Semal, P., van der Plicht, J.,

Bocherens, H., Krause, J., 2016. Neandertal cannibalism and Neandertal bones used as tools in Northern Europe. Sci. Rep. 6, 29005.

Ruff, C.B., Trinkaus, E., Holliday, T.W., 1997. Body mass and encephalization in Pleistocene *Homo*. Nature 387, 173–176.

Sala, N., Conard, N., 2016. Taphonomic analysis of the hominin remains from Swabian Jura and their implications for the mortuary practices during the Upper Paleolithic. Quatern. Sci. Rev. 150, 278–300.

Sala, N., Arsuaga, J.L., Martínez, I., Gracia-Téllez, A., 2014. Carnivore activity in the Sima de los Huesos (Atapuerca, Spain) hominin sample. Quatern. Sci. Rev. 97, 71–83.

Sala, N., Arsuaga, J.L., Martínez, I., Gracia-Téllez, A., 2015a. Breakage patterns in Sima de los Huesos (Atapuerca, Spain) hominin sample. J. Archaeol. Sci. 55, 113–121.

Sala, N., Arsuaga, J.L., Pantoja-Pérez, A., Pablos, A., Martínez, I., Quam, R.M., Gómez-Olivencia, A., Bermúdez de Castro, J.M., Carbonell, E., 2015b. Lethal Interpersonal Violence in the Middle Pleistocene. PLoS One 10, e0126589.

Sala, N., Pantoja-Pérez, A., Arsuaga, J.L., Pablos, A., Martínez, I., 2016. The Sima de los Huesos Crania: Analysis of the cranial breakage patterns. J. Archaeol. Sci. 72, 25–43.

Saladié, P., Huguet, R., Rodríguez-Hidalgo, A., Cáceres, I., Esteban-Nadal, M., Arsuaga, J.L., Bermúdez de Castro, J.M., Carbonell, E., 2012. Intergroup cannibalism in the European Early Pleistocene: The range expansion and imbalance of power hypotheses. J. Hum. Evol. 63, 682–695.

Spoor, F., Wood, B., Zonneveld, F., 1994. Implications of early hominid labyrinthine morphology for evolution of human bidepal locomotion. Nature. 369, 645–648.

Stoessel, A., Gunz, P., David, R., Spoor, F., 2016a. Comparative anatomy of the middle ear ossicles of extant hominids—Introducing a geometric morphometric protocol. J. Hum. Evol. 91, 1–25.

Stoessel, A., David, R., Gunz, P., Schmidt, T., Spoor, F., Hublin, J.-J., 2016b. Morphology and function of Neandertal and modern human ear ossicles. Proc. Natl. Acad. Sci. 113, 11489–11494.

Todd, T.W., 1920. Age changes in the pubic bone: I. The white male pubis. Am. J. Phys. Anthropol. 3, 467–470.

Trinkaus, E., 1985. Pathology and the posture of the La Chapelle-aux-Saints Neandertal. Am. J. Phys. Anthropol. 67, 19–41.

Trinkaus, E., Churchill, S.E., Ruff, C.B., 1994. Postcranial robusticity in *Homo*. II: humeral bilateral asymmetry and bone plasticity. Am. J. Phys. Anthropol. 93, 1–34.

Turq, A., Dibble, H., Goldberg, P., McPherron, S.J.-P., Sandgathe, D., Mercier, N., Brüxelles, L., Laville, D., Madelaine, S., 2012. Reprise des fouilles das la partie ouest du gisement de la Ferrassie, Savignac-de-Miremont, Dordogne : problématique et premiers résultats. In: Bertran, P., Lenoble, A. (Eds.), Quaternaire continental d'Aquitaine: un point sur les travaux récents. Excursion AFEQ-ASF 30 mai-01 juin 2012. ASF-AFEQ, Bordeaux, pp. 78–87.

Ubelaker, D.H., Adams, B.J., 1995. Differentiation of perimortem and postmortem trauma using taphonomic indicators J. For. Sci. 40, 509–512.

Val, A., 2016. Deliberate body disposal by hominins in the Dinaledi Chamber, Cradle of Humankind, South Africa? J. Hum. Evol. 96, 145–148.

Vandermeersch, B., Trinkaus, E., 1995. The postcranial remains of the Regourdou 1 Neandertal: the shoulder and arm remains. J. Hum. Evol. 28, 439–476.

Villa, P., Mahieu, E., 1991. Breakage patterns of human long bones. J. Hum. Evol. 21, 27–48.

Voisin, J.-L., 2006. Krapina and other neanderthal clavicles: a peculiar morphology? Period. Biol. 108, 331–339.

Wedel, V.L., Galloway, A., 2014. Broken bones: Anthropological analysis of blunt force trauma. Charles C. Thomas, Springfield.

Wever, E., Lawrence, M., 1954. Physiological Acoustics. Princeton University Press, Princeton.

Figure legends

Figure 1. Virtual reconstruction of the ear ossicles found in the right temporal bone of the La Ferrassie 1 Neandertal skeleton (see also SOM Fig. S2).

Figure 2. Recently identified new vertebral fossils belonging to La Ferrassie 1. Left lateral (a1) and dorsal (a2) views of a thoracic (T5-T8) vertebral body fragment preserving part of the pedicle (see the represented part on Kebara 2's T4 3D virtual reconstruction in lateral view). Medial (b1) and dorsal (b2) views of the upper right articular facet of a thoracic vertebra (see the represented part on Kebara 2's T9 3D virtual reconstruction in dorsal view). Ventral (c1) and caudal (c2) views of a fragment of lumbar vertebral body (L5?) and the represented part on Kebara 2's L5 3D virtual reconstruction.

Figure 3. New costal remains belonging to the LF1 skeleton. External (a1) and internal (a2) views of a fragment of a left rib preserving the neck and the articular tubercle (a. tb.). External (b1) and internal (b2) views of a shaft fragment of a rib of indeterminate side preserving the costal groove (c. gr.).

Figure 4. Cranial (a) and caudal (b, d) views of the La Ferrassie 1 (LF1) and caudal view of the atlas of Krapina CA1.98 (c). In d, the wrongly reconstructed right half of the posterior arch has been "virtually" placed in its proper place using imaging software. Note the size difference between the transverse foramen of LF1 compared to the Krapina specimen. Also note the large asymmetry of the vertebral foramen of LF1. In our view, the groove on the left side is due to the left vertebral artery that entered the spinal canal of the C1 directly from the transverse process of the C2, rather than passing

through the C1 transverse process.

Figure 5. Selected pathological lesions of the vertebral column of LF1. Ventral view of #3 (C3) of La Ferrassie 1 (a and b); note the difference in the height of the articular pillars and on the uncinate processes. Dorsal view of the fifth lumbar and sacrum of La Ferrassie 1 (c and d). The arrows indicate remodeling of the bone surface because of the contact between the L5 and the sacrum (lower left arrow) or between the L4 and L5 (upper central and right arrows). This remodeling occurs on the left side of these bones, which indicates a concavity of the spine to the left. Note also the clockwise rotation of the spinous process (Gómez-Olivencia, 2013) that would be consistent with the concavity to the left of the spine.

Figure 6. Left sixth or seventh rib of La Ferrassie 1: internal (a), cranio-external (b), and caudal (c, d) views; 3D reconstruction and transverse (1, 8) and cross-sections (2–7). The asterisk indicates a protruding small bone chip (see text). b1 = bulge 1, b2 = bulge 2, s = adhered sediment. Scale bars represent 1 cm.

Figure 7. Comparison between the clavicles of La Ferrassie 1. For a better comparison, we have mirror-imaged the right side. The two clavicles look similar in cranial view, except for the shape of the attachment of the deltoid muscle. In contrast, there is a pronounced difference in dorsal view between the two clavicles. The arrows indicate "bumps" of the diaphysis on the left side clavicle.

Figure 8. 3D reconstruction of the left clavicle of La Ferrassie 1, showing different sections (numbers 1 to 8). Letters "A" and "B" indicate recent (postdepositional) fractures of the bone. The asterisk indicates the area of interest in which the density and

arrangement of the trabeculae is different from the clavicle of the right side (compare with Fig. 9).

Figure 9. 3D reconstruction of the right clavicle of La Ferrassie 1, showing different sections (numbers 1 to 5). Letters “A” and “B” indicate recent (postdepositional) fractures of the bone. The arrangement of the trabeculae in this clavicle looks normal and more organized than its left side counterpart (see Fig. 8).

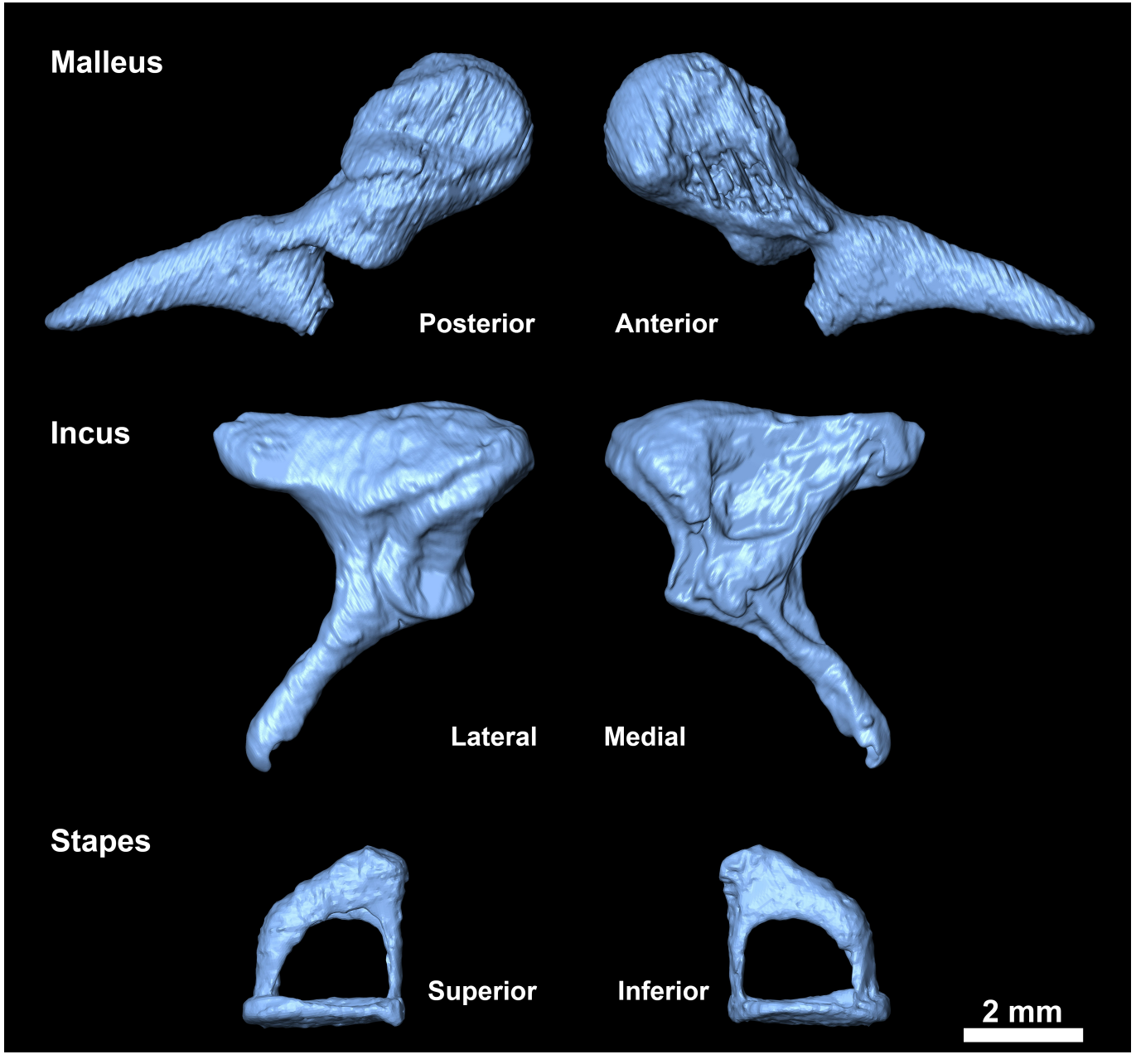
Malleus
Posterior
Anterior
Incus
Lateral
Medial
Stapes
Superior
Inferior
2 mm

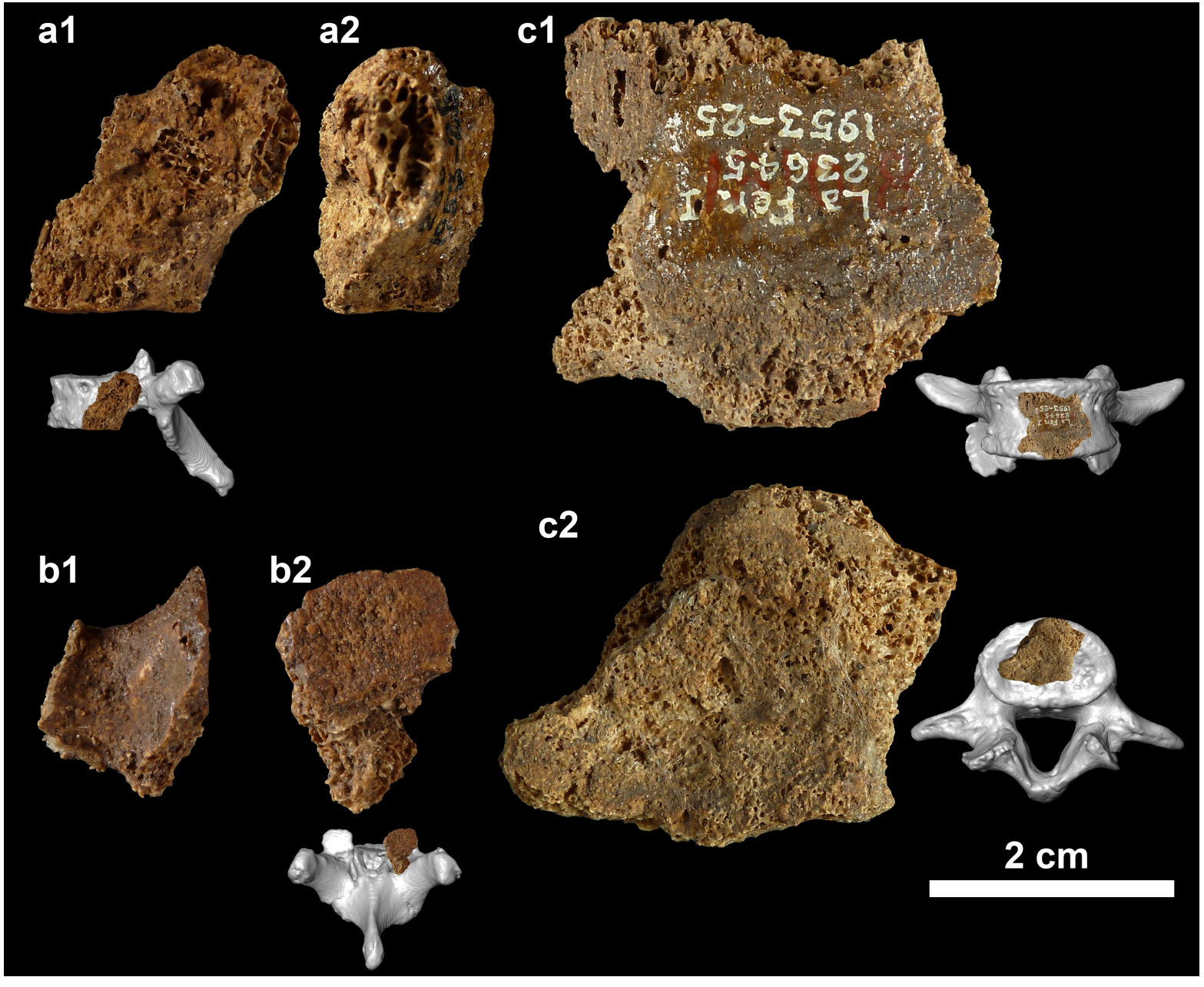
a1
a2
c1
b1
b2
c2
2 cm

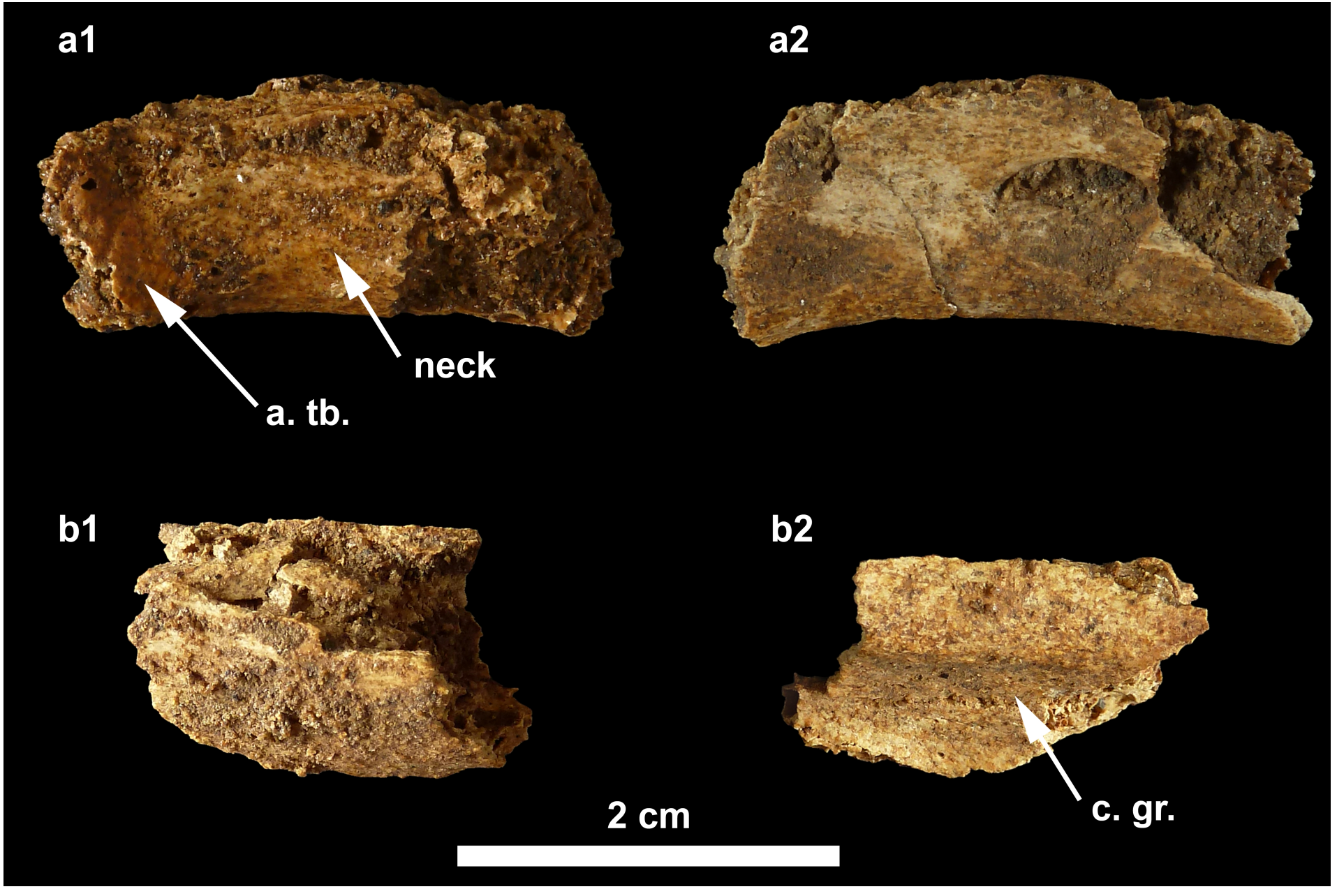
a1
a2
neck
a. tb.
b1
b2
c. gr.
2 cm

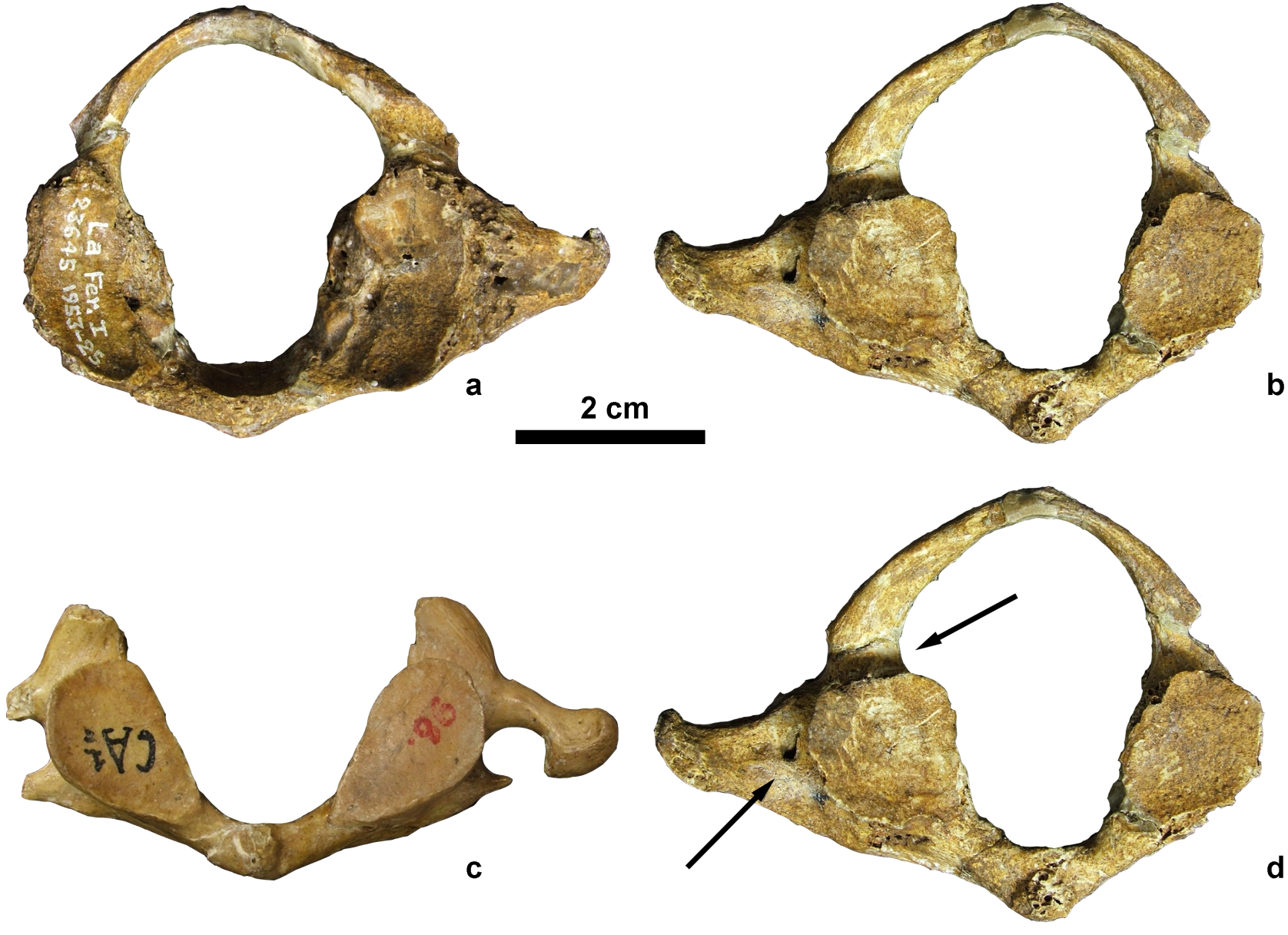
a
b
2 cm
c
d

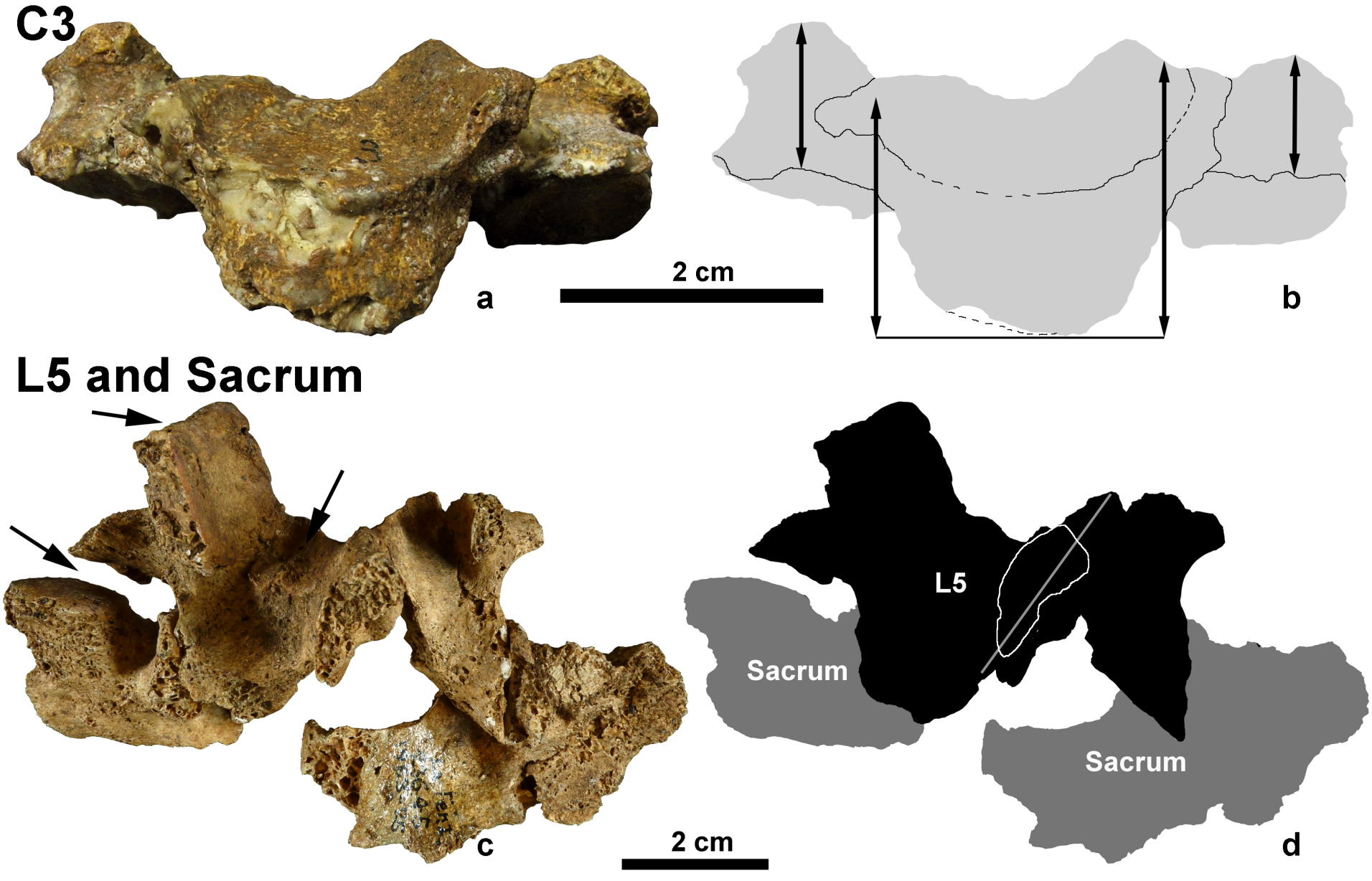
C3
a
2 cm
b
L5 and Sacrum
c
2 cm
L5
Sacrum
Sacrum
d

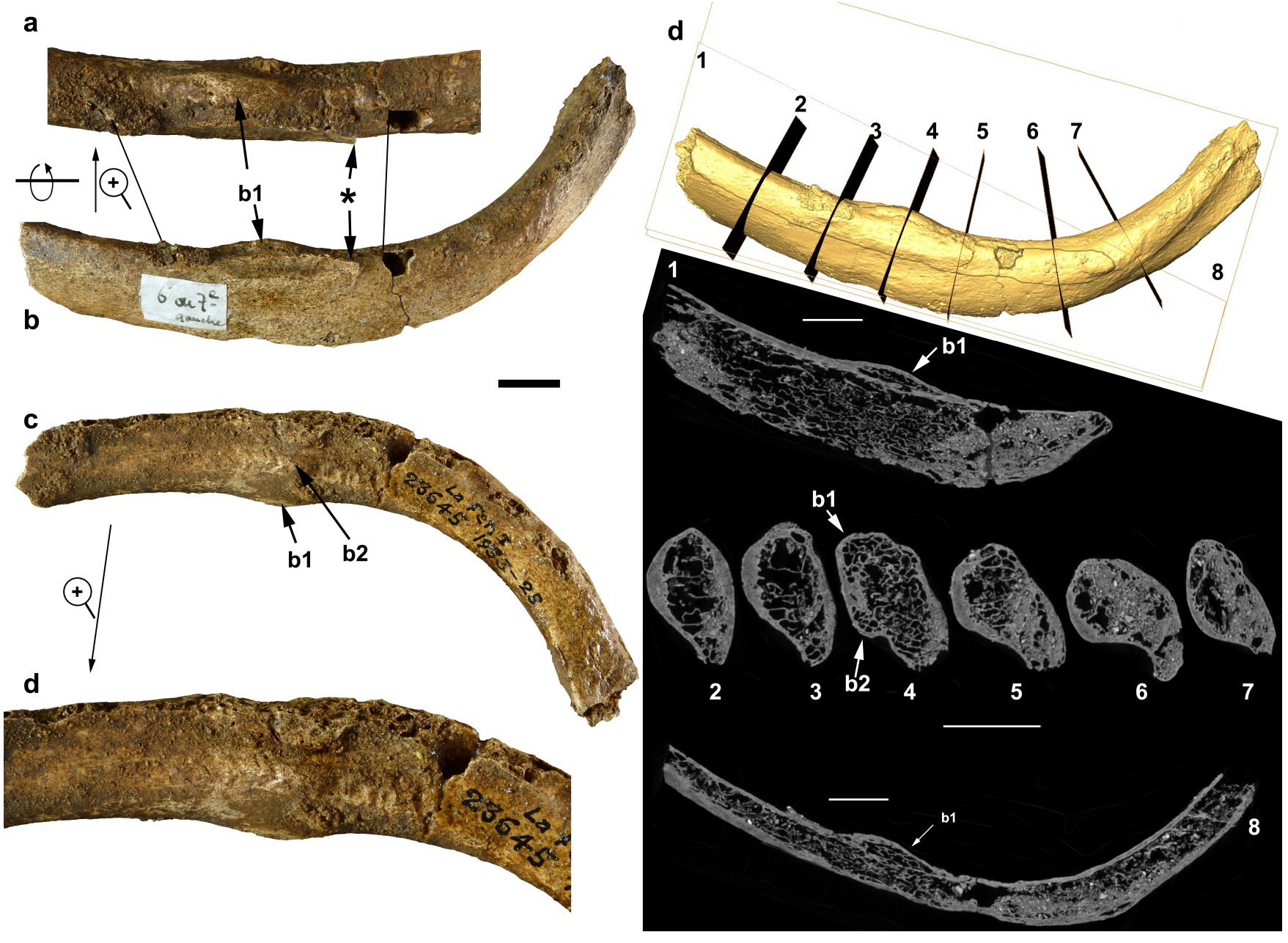
a
b1
*
b
c
b1
b2
d
d
1
2
3
4
5
6
7
8
b1
b1
b2
2
3
4
5
6
7
b1
8

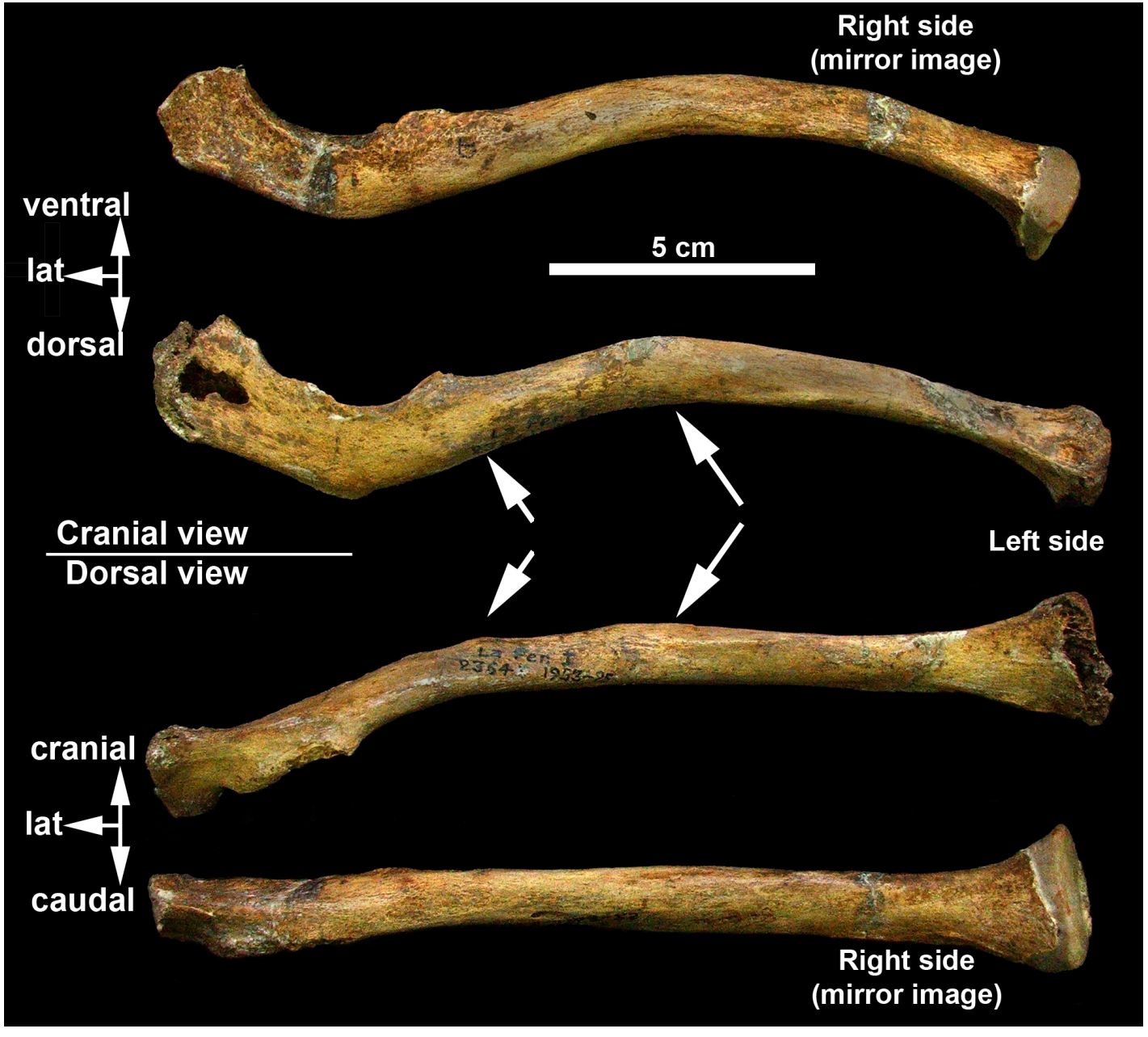
Right side
(mirror image)
ventral
lat
dorsal
5 cm
Cranial view
Dorsal view
Left side
cranial
lat
caudal
Right side
(mirror image)

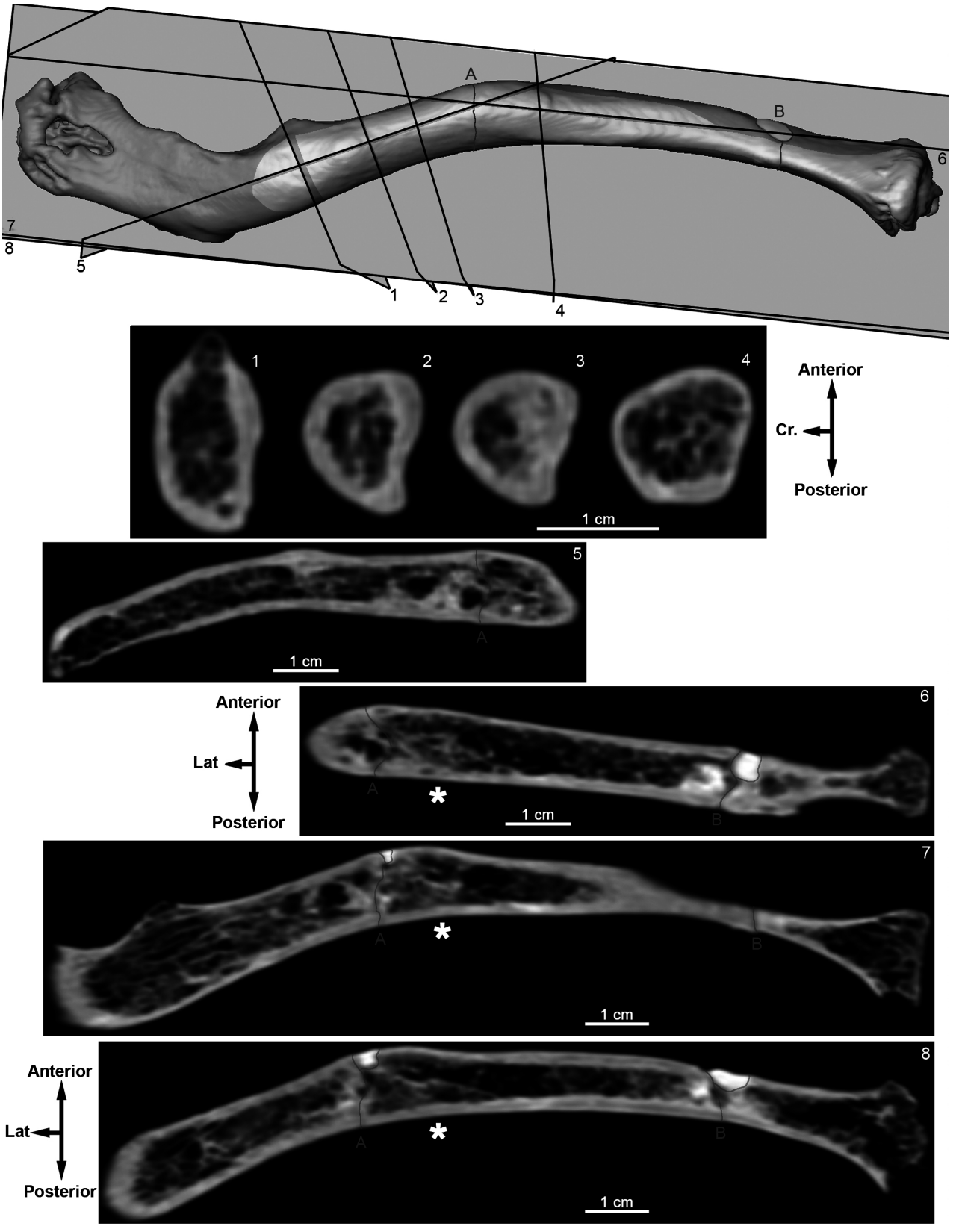
A
B
6
7
8
5
1
2
3
4
1
2
3
4
Anterior
Cr.
Posterior
1 cm
5
A
1 cm
Anterior
Lat
Posterior
6
A
*
1 cm
B
7
A
*
1 cm
B
Anterior
Lat
Posterior
8
A
*
1 cm
B

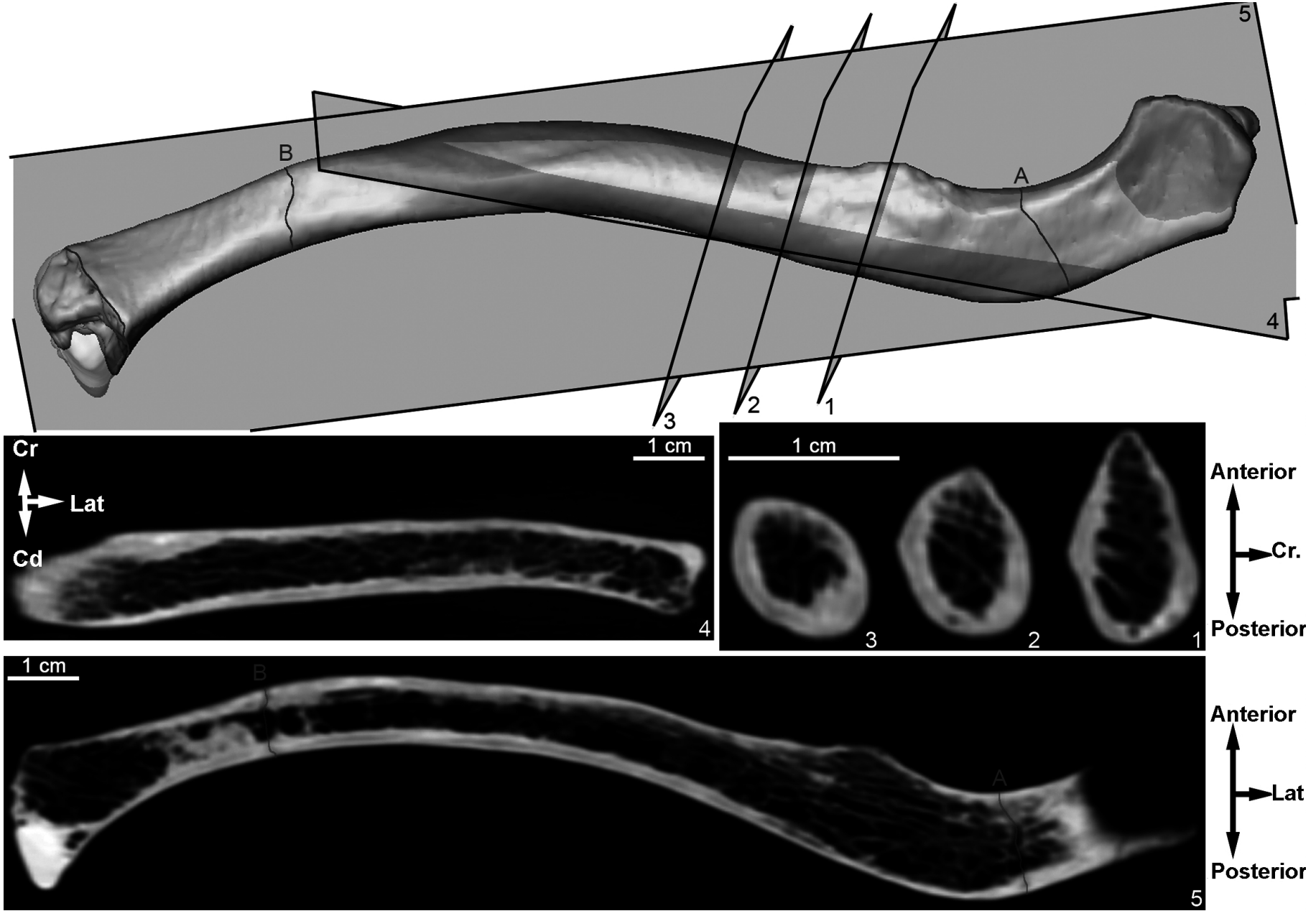
5
B
A
4
3
2
1
Cr
Lat
Cd
1 cm
4
1 cm
3
2
1
Anterior
Cr.
Posterior
1 cm
B
A
5
Anterior
Lat
Posterior

Table 1

Raw dimensions of the La Ferrassie 1 malleus, summary statistics of other fossils, recent and fossil modern human samples, and results of the z-score analysis between Neandertals and recent modern humans.[a]

Specimen/Sample	Total length (mm)	Manubrium length (mm)	Manubrium ML thickness (mm)	Manubrium arc depth (mm)	Length of the corpus (mm)	S-I head width (mm)	Angle between the axes (º)	Source
La Ferrassie 1	8.78	4.90	1.10	0.49	6.26	2.60	140.6	This study
La Ferrassie 3		4.89	**1.26***	0.44		**2.92****		Quam et al., 2013b
Neandertals mean ± s.d.	8.56 ± 0.36							Stoessel et al., 2016a
Neandertals range (*n*)	8.23–8.96 (4)							
Mid. Pleist. Europe range (*n*)	8.80–8.98 (2)	5.16 (1)			6.40 (1)	2.70 (1)		Martínez et al., 2004; Crevecoeur, 2007; Stoessel et al., 2016a
Fossil *H. sapiens* mean ± s.d.	7.84 ± 0.23	4.49 ± 0.27	0.95 ± 0.13	0.24 ± 0.09	5.42 ± 0.18	2.45 ± 0.12	137.4 ± 3.2	Original specimens; Lisoněk and Trinkaus, 2006
Fossil *H. sapiens* range (*n*)	7.37–8.10 (8)	4.02–4.80 (6)	0.81–1.10 (4)	0.14–0.33 (4)	5.21–5.67 (7)	2.30–2.62 (7)	132.1–140.0 (5)	Crevecoeur, 2007; Ponce de León and Zollikofer, 2013
Recent *H. sapiens* mean ± s.d.	8.25 ± 0.41	4.94 ± 0.31	1.00 ± 0.09	0.33 ± 0.15	5.83 ± 0.35	2.43 ± 0.17	132.1 ± 6.2	Quam, 2006
Recent *H. sapiens* range (*n*)	7.43–9.31 (43)	4.22–5.59 (43)	0.81–1.28 (43)	0.05–0.64 (43)	4.96–6.69 (43)	2.03–2.79 (43)	116.5–145.7 (43)	

[a] Values underlined are outside the range of the modern human comparative sample. The fossil remains with a * or ** are significantly different from the modern comparative sample based on a z-score analysis (*$p < 0.05$, **$p < 0.01$). Values in bold indicate those values that are significantly different and/or outside of the range of the modern human sample.

Table 2

Raw dimensions of the La Ferrassie 1 incus, summary statistics of other fossils, recent and fossil modern human samples, and results of the z-score analysis between Neandertals and recent modern humans.[a]

Specimen/Sample	Short process length (mm)	Long process length (mm)	Functional length (mm)	Long process arc depth (mm)	Articular facet height (mm)	Inter-process length (mm)	Inter-process arc depth (mm)	Angle between the axes (º)	Incudal index	Source
La Ferrassie 1	5.26	7.22	4.25	0.55	**3.50****	5.71	1.81	**53.7***	72.9	This study
La Ferrassie 3	4.74	6.89	4.08	0.40	3.34	**5.51***	1.43	**48.2****	68.8	Quam et al., 2013b
Amud 7	5.07	6.98	4.08	**0.28****	**3.44***	**5.38***	**2.13***	**48.3****	72.6	Quam and Rak, 2008
Neandertal sample (mean ± s.d)		7.25 ± 0.28								Stoessel et al., 2016a
Neandertals range (*n*)		6.74–7.58 (10)								
Mid. Pleist. Europe range (*n*)	4.90 (1)	7.50–7.69 (2)	4.33 (1)			5.90 (1)				Martínez et al., 2004; Lisoněk and Trinkaus, 2006; Crevecoeur, 2007
Fossil *H. sapiens* (mean ± s.d)	4.76 ± 0.44	6.61 ± 0.29	3.90 ± 0.19	0.38 ± 0.10	3.23 ± 0.15	5.79 ± 0.44	1.58 ± 0.27	61.3 ± 4.9	71.3 ± 4.5	Lisoněk and Trinkaus, 2006; Crevecoeur, 2007; Quam et al., 2013b; Stoessel et al., 2016a
Fossil *H. sapiens* range (*n*)	4.10–5.50 (7)	6.30–7.10 (8)	3.57–4.11 (6)	0.26–0.56 (7)	2.99–3.45 (7)	5.29–6.60 (6)	1.30–2.00 (6)	52.4–67.3 (7)	64.1–77.5 (6)	
Recent *H. sapiens* (mean ± s.d)	5.07 ± 0.37	6.83 ± 0.32	4.00 ± 0.21	0.56 ± 0.14	3.00 ± 0.19	6.18 ± 0.34	1.66 ± 0.21	64.0 ± 4.7	74.3 ± 4.9	Quam, 2006
Recent *H. sapiens* range (*n*)	4.02–5.86 (41)	6.17–7.59 (43)	3.61–4.46 (42)	0.25–0.80 (43)	2.60–3.41 (42)	5.61–7.44 (41)	1.18–1.95 (41)	56.6–75.6 (41)	59.2–84.8 (41)	

[a]Values underlined are outside the range of the modern human comparative sample. The fossil remains with a * or ** are significantly different from the modern comparative sample based on a z-score analysis (*$p < 0.05$, **$p < 0.01$). Values in bold indicate those values that are significantly different and/or outside of the range of the modern human sample.

Table 3

The middle ear lever ratio[a] in La Ferrassie 1 and Pleistocene and recent hominins.[a]

Specimen/Sample	Malleus functional length (mm)	Incus functional length (mm)	Middle Ear lever ratio[b]	Source
Mid. Pleist. Europe (*n* = 1)	5.16	4.33	119.2	Martínez et al., 2004
La Ferrassie 1	4.90	4.25	115.3	This study
La Ferrassie 3	4.89	4.08	119.9	Quam et al., 2013b
Neandertals mean ± s.d.			116.0 ± 10.0	Stoessel et al., 2016a
Neandertals range (*n*)			105.0–125.0 (5)	
Qafzeh 12	**4.02****	3.84	**104.7***	Quam and Rak, 2008
Qafzeh 15	4.48	**3.57***	125.5	Quam and Rak, 2008
Dolní Věstonice 14	4.60	4.11	111.9	Lisoněk and Trinkaus, 2006
Recent *H. sapiens* (mean ± s.d)	4.94 ± 0.31	4.00 ± 0.21	123.4 ± 8.5	Quam, 2006
Recent *H. sapiens* range (*n*)	4.22–5.59 (43)	3.61–4.46 (42)	101.9–138.9 (42)	
Recent *H. sapiens* (mean ± s.d)			120.1 ± 8.4	Stoessel et al., 2016a
Recent H. sapiens range (*n*)			107.7–137.0 (27)	

[a]Values underlined are outside the range of the modern human comparative sample. The fossil remains with a * or ** are significantly different from the modern comparative sample based on a z-score analysis (*$p < 0.05$, **$p < 0.01$). Values in bold indicate those values that are significantly different and/or outside of the range of the modern human sample.

[b] Lever ratio = (Malleus functional length/Incus functional length) × 100

Table 4

Raw dimensions of the La Ferrassie 1 stapes, summary statistics of other fossils, recent and fossil modern human samples, and results of the z-score analysis between Neandertals and recent modern humans.[a]

Specimen/Sample	Head	Total	Foramen	Obturatorforamen width (mm)	Anterior crus length (mm)	Posterior crus length (mm)	Angle A (º)	Angle B (º)	Angle C (º)	Stapedial index	Source
La Ferrassie 1	1.05	3.04	1.65	1.98	2.56	3.29	52.1	78.3	49.6	90.1	This study
La Ferrassie 3	**0.71****	2.76	1.89	1.79	2.38	3.20	47.3	86.9	45.7	90.6	Quam et al., 2013b
La Ferrassie 8	**0.80***	2.63	1.75	1.74	2.60	3.20	48.3	89.7	42.0	83.3	Gómez-Olivencia et al., 2015
Subalyuk 2	0.93	(2.70)	(1.60)	1.60	(2.45)	(2.90)	(50.3)				Quam et al., 2013b
Neandertal sample (mean ± s.d)		3.11 ± 0.18									Stoessel et al., 2016a
Neandertal sample range		2.88–3.31									
(*n*)		(5)									
Oase 2					(3.2)	(3.0)					Ponce de León and Zollikofer, 2013
Cro-Magnon 1		3.39									Stoessel et al., 2016a
Recent *H. sapiens* (mean ± s.d.)	1.21 ± 0.16	3.44 ± 0.20	1.90 ± 0.18	1.74 ± 0.19	3.40 ± 0.21	3.35 ± 0.20	49.7 ± 3.4	67.4 ± 3.5	63.0 ± 4.1	85.90 ± 5.29	Quam, 2006
Recent *H. sapiens* range	0.84–1.52	2.94–3.87	1.52–2.30	1.34–2.18	2.94–3.93	2.77–3.72	44.3–59.6	60.4–75.0	53.6–70.3	77.20–102.72	
(*n*)	(40)	(40)	(41)	(42)	(40)	(40)	(40)	(40)	(40)	(39)	

[a]Values in parentheses are estimated. Values underlined are outside the range of the modern human comparative sample. The fossil remains with a * or ** are significantly different from the modern comparative sample based on a z-score analysis (* = $p < 0.05$, ** = $p < 0.01$). Values in bold indicate those values that are significantly different and/or outside of the range of the modern human sample.

Table 5
Comparison of stapes footplate and oval window dimensions in the La Ferrassie 1 Neandertal compared to other Neandertals, Middle Pleistocene fossils, and recent and fossil modern humans.[a]

Specimen/Sample	Footplate length (mm)	Footplate width (mm)	Measured footplate area (mm^2)	Measured oval window area (mm^2)	Footplate index	Oval window index	Source
La Ferrassie 1	2.74	1.49	3.39		**54.4***		Original specimen
La Ferrassie 3	**(2.50)****	(1.25)		2.70	(50.0)	54.0	Original specimen
La Ferrassie 8	**2.19****	1.22	**2.16****		**55.7***		Gómez-Olivencia et al., 2015
Neandertals (mean ± s.d.)			2.58 ± 0.20	3.01 ± 0.35		54.6 ± 1.6	Quam et al., 2013b; Stoessel et al., 2016a
Neandertals range (*n*)			2.35–2.81 (5)	2.36–3.67 (18)		53.2–56.5 (5)	
Mid. Pleist. Europe range (*n*)			2.77 (1)	3.02–3.98 (3)			Martínez et al., 2004
Oase 2	2.9						Ponce de León and Zollikofer, 2013
Cro Magnon 1			2.99				Stoessel et al., 2016a
Fossil *H. sapiens* (mean ± s.d)				3.46 ± 0.28		48.8 ± 5.8	Quam et al., 2013b
Fossil *H. sapiens* range (*n*)				3.06–3.88 (9)		36.7–55.8 (9)	
Recent *H. sapiens* (mean ± s.d)	2.94 ± 0.14	1.39 ± 0.10	3.39 ± 0.32		47.29 ± 3.30		Original specimens
Recent *H. sapiens* range (*n*)	2.47–3.27 (46)	1.20–1.63 (43)	2.95–4.29 (41)		40.27–57.09 (43)		

[a]Values in parentheses are estimated. Values underlined are outside the range of the modern human comparative sample. The fossil remains with a * or ** are significantly different from the modern comparative sample based on a z-score analysis (*$p < 0.05$, **$p < 0.01$).Values in bold indicate those values that are significantly different and/or outside of the range of the modern human sample.

Table 6
Fracture properties in the La Ferrassie 1 long bones.

		NISP[a]	%
Fracture outline	Longitudinal	0	0.0
	Transversal	16	80.0
	Oblique	4	20.0
Fracture angle	Right	11	100.0
	Acute/obtuse	0	0.0
	Mixed	0	0.0
Fracture edge	Smooth	0	0.0
	Jagged	17	100.0
	Mixed	0	0.0
Shaft circumference	1: < 50%	0	0.0
	2: > 50%	0	0.0
	3: Complete	18	100.0
Shaft fragment	1: <25%	0	0.0
	2: 25-50%	1	5.6
	3: 50-75%	3	16.7
	4: >75%	14	77.8

[a]NISP = Number of identified specimens

Table 7
Results of the chi square analysis of the fracture properties of La Ferrassie 1 compared to other samples[a].

Long bones	Fracture angle	Fracture outline	Shaft circumference
LF1 vs Sarrians	*n* (11/269) Chi^2 = 5.6943 *p* = 0.058	*n* (20/326) Chi^2 = 5.0299 *p* = 0.081	*n* (18/226) Chi^2 = 2.3178 *p* = 0.314
LF1 vs Fontbrégoua	*n* (11/174) Chi^2 = 25.609 *p* = **2.75E-06**	*n* (20/169) Chi^2 = 6.36 *p* = **0.041586**	*n* (18/151) Chi^2 = 89.681 *p* = **3.36E-20**
LF1 vs SH	*n* (11/471) Chi^2 = 1.3907 *p* = 0.499	*n* (20/587) Chi^2 = 1.4454 *p* = 0.485	*n* (18/475) Chi^2 = 1.3839 *p* = 0.501

Cranial bones	Fracture angle	Cortical delamination
LF1 vs SH	N (25/513) Chi^2 = 0.88016 *p* = 0.348	N (25/518) Chi^2 = 1.2648 *p* = 0.261
LF1 vs Agris	N (25/15) Chi^2 = 25.378 *p* = **4.71E-07**	N (25/15) Chi^2 = 35.897 *p* = **2.08E-09**
LF1 vs AUZAI	N (25/46) Chi^2 = 40.888 *p* = **1.61E-10**	N (25/46) Chi^2 = 11.225 *p* = **0.00081**
LF1 vs Corconne	N (25/297) Chi^2 = 1.3527 *p* = 0.245	N (25/297) Chi^2 = 3.8446 *p* = 0.050
LF1 vs Villedubert	N (25/1760) Chi^2 = 1.6228 *p* = 0.203	N (25/1760) Chi^2 = 3.5643 *p* = 0.059
LF1 vs LC1	N (25/16) Chi^2 = 3.7028 *p* = 0.054	N (26/17) Chi^2 = 0.096099 *p* = 0.757
LF1 vs LQH5	N (25/30) Chi^2 = 0.056122 *p* = 0.813	N (26/31) Chi^2 = 0.016073 *p* = 0.899

[a]Bold *p*-values refer to significant results. Data for LF1 (La Ferrassie 1), LC1 (La Chapelle-aux-Saints 1), and LQH5 (La Quina H5) are original from this work. In the all other cases, it has been extracted from the bibliography: Sarrians and Fontbrégoua Neolithic assemblages from Villa and Mahieu (1991); Agris Mesolithic site, AUZAI (Châteliers du Vieil-Auzay from the Neolithic period), the Neolithic site of Corconne site and the Chalcolithic site of Villedubert from Jordana et al. (2013); and SH (Sima de los Huesos Middle Pleistocene hominins) from Sala et al. (2015a, 2016). Fontbrégoua, Agris and Châteliers du Vieil-Auzay are considered typically fresh bone fractured samples. Sarrians, Corconne, Villedubert and Sima de los Huesos are considered samples with dry bone fractures pattern.

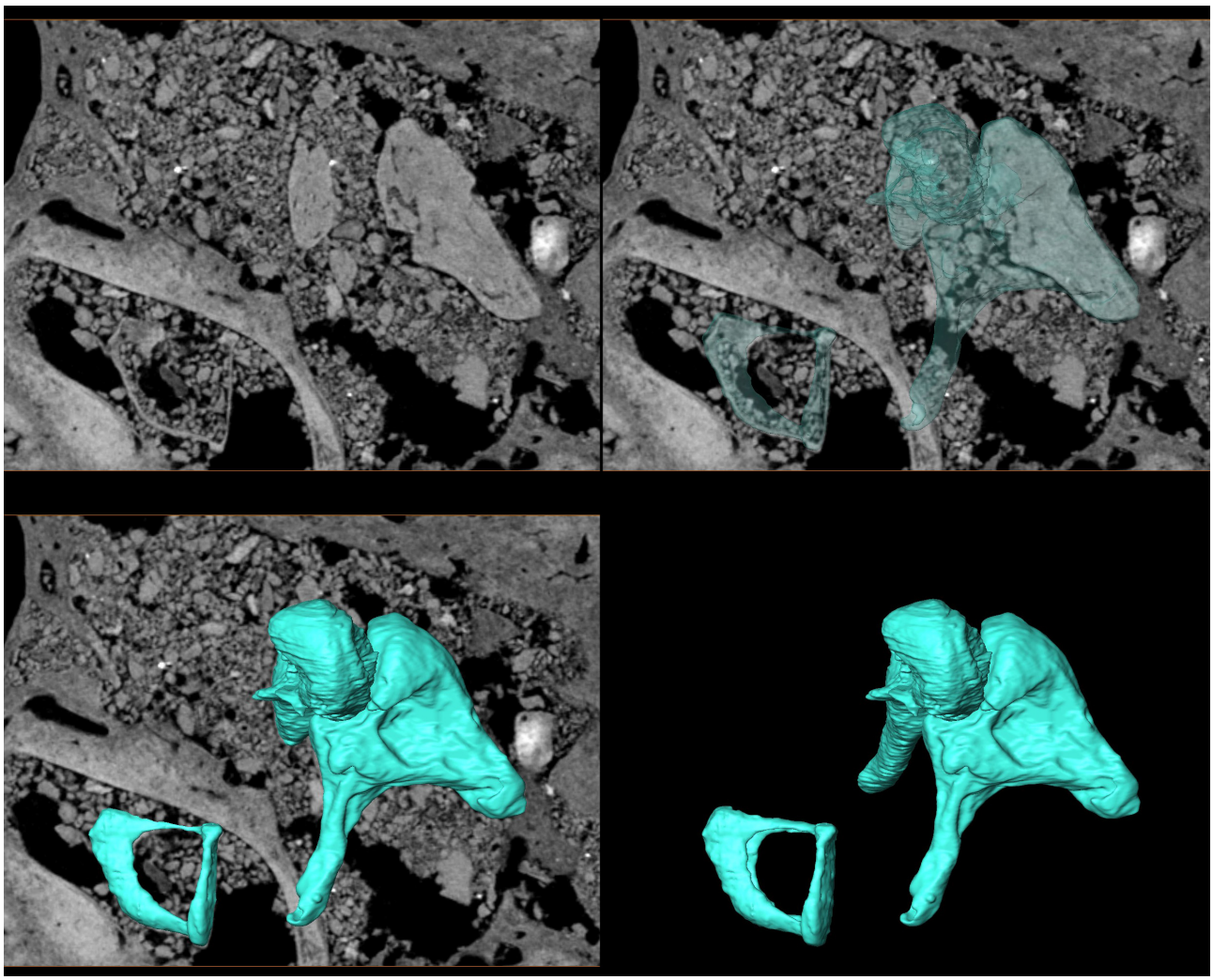

SOM Figure S1. Cross-section of the right temporal bone of La Ferrassie 1 Neandertal showing the position of the three ear ossicles and their 3D virtual reconstructions.

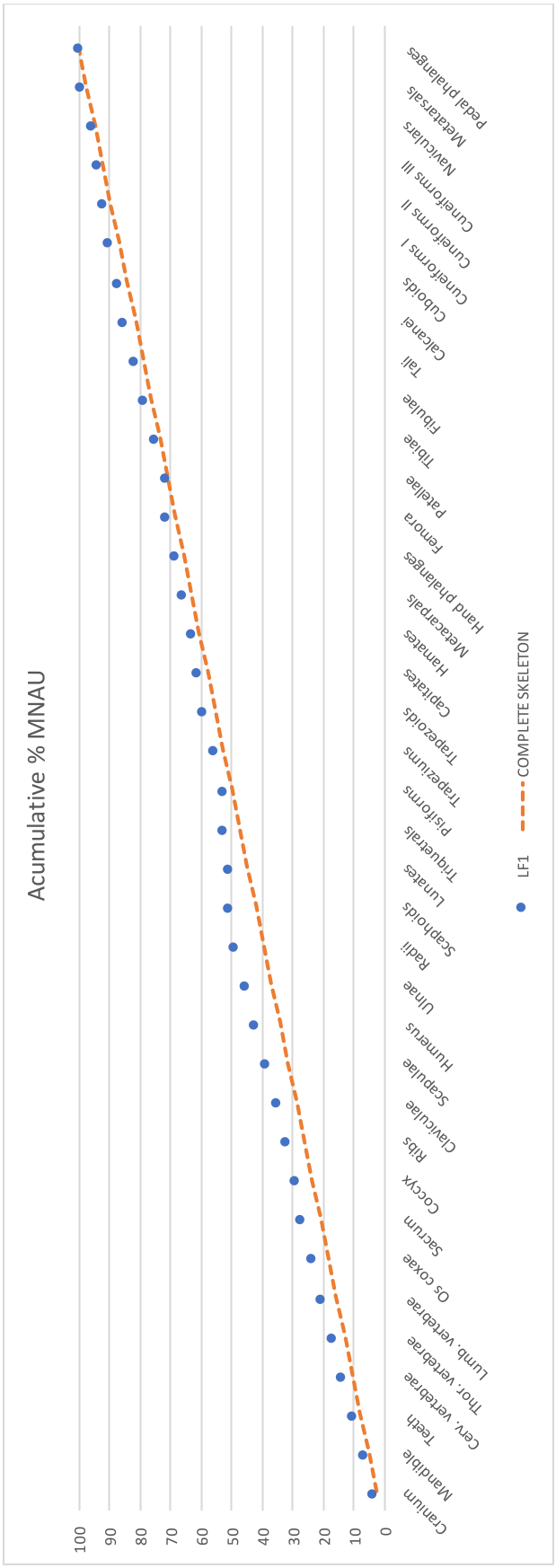

SOM Figure S2. Cumulative percentage of the minimum number of anatomical units (MNAU), i.e., number of bones or bone portions preserved in a sample divided by number of that bone or bone portion in a complete skeleton, present in La Ferrassie 1 (blue dots) compared to what would be expected in a complete skeleton (orange line; see SOM Table S1).

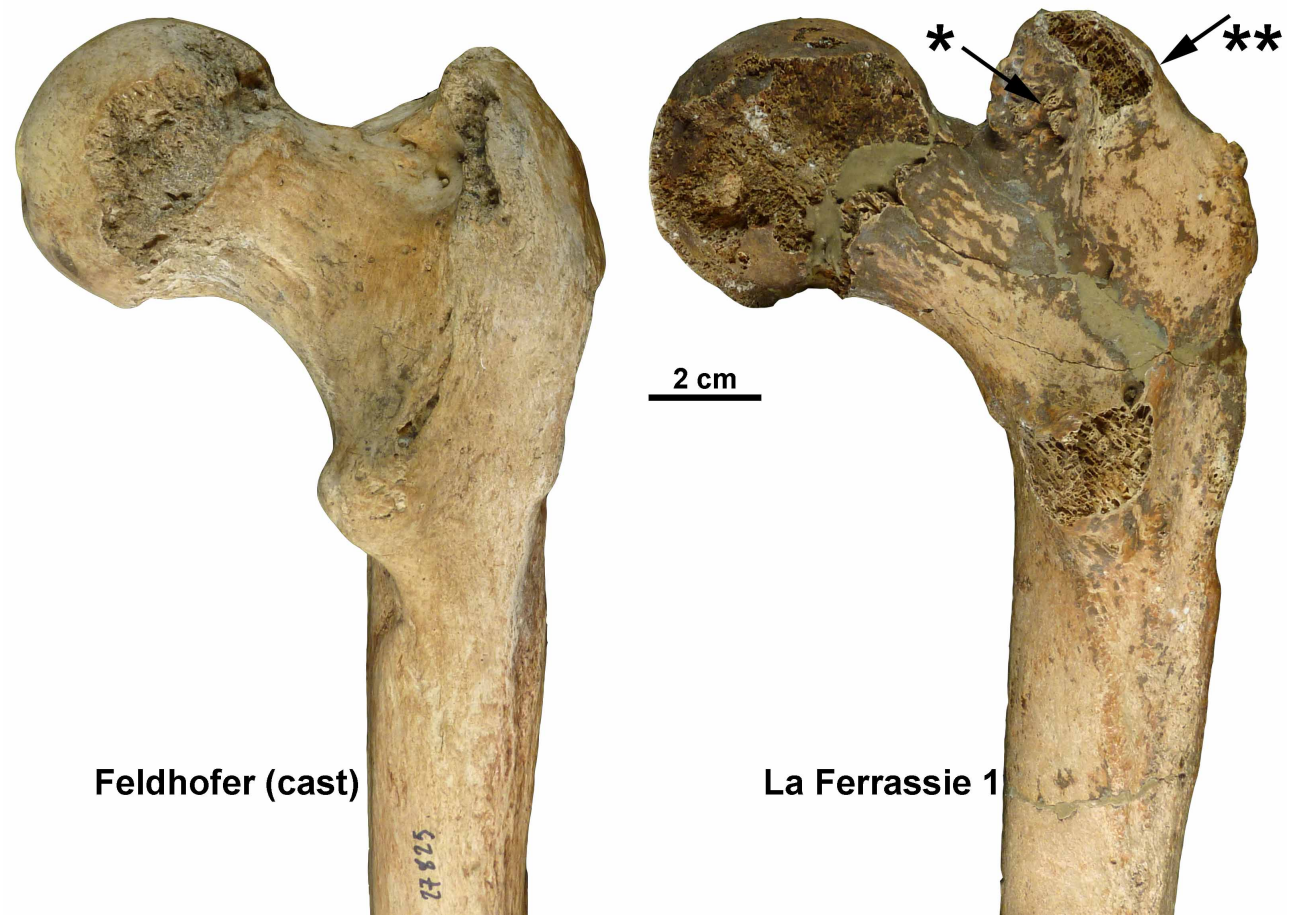

SOM Figure S3. Dorsal view of the cast of the right femur of the Feldhofer Neandertal (left) with the right femur of the La Ferrassie 1 Neandertal. Note the difference in the size and location of the greater trochanter (arrow with **). Note also the exostosis present in the trochanteric fossa (arrow with *).

SOM Figure S4. Left ulna of the La Ferrassie 1 Neandertal skeleton: original bone and 3D reconstruction in ventral (anterior) views (left half of the image) and longitudinal section and detail of the section from the CT-scan showing two natural bone fractures with angles close to 90º (right half of the image).

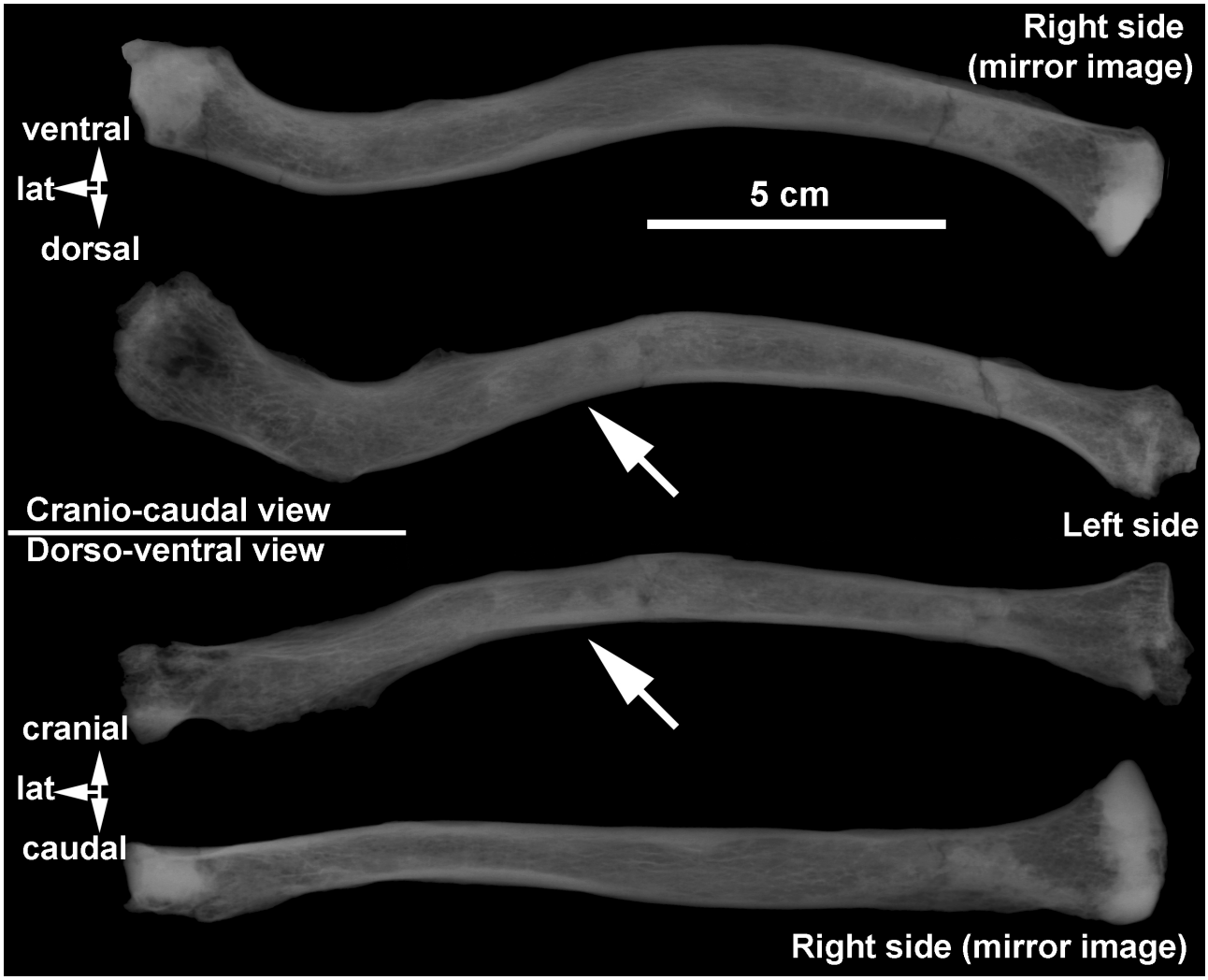

SOM Figure S5. Cranio-caudal and dorso-ventral x-rays of the clavicles of La Ferrassie 1. Note the difference in the trabecular organization in the shaft, which is more irregular in the left clavicle (arrows).

SOM Table S1
Anatomical representation (absolute and relative) of the La Ferrassie 1 individual and cumulative percentage.

Anatomical region	NISP	NME	N°AU	One skeleton	MNAU	Relative MNAU	Cumulative % MNAU
Cranium	>25	1	1	1	1.00	3.41	3.41
Mandible	6	1	1	1	1.00	3.41	6.83
Teeth	32	32	32	32	1.00	3.41	10.24
Cerv. vertebrae	7*	7	7	7	1.00	3.41	13.65
Thor. vertebrae	18*	11	11	12	0.92	3.13	16.78
Lumb. vertebrae	9*	5	5	5	1.00	3.41	20.19
Os coxae	3	2	2	2	1.00	3.41	23.61
Sacrum	3	1	1	1	1.00	3.41	27.02
Coccyx	1	1	1	2	0.50	1.71	28.73
Ribs	43*	22**	22	24	0.92	3.13	31.85
Claviculae	5	2	2	2	1.00	3.41	35.27
Scapulae	7	2	2	2	1.00	3.41	38.68
Humerus	3	2	2	2	1.00	3.41	42.09
Ulnae	4	2	2	2	1.00	3.41	45.51
Radii	3	2	2	2	1.00	3.41	48.92
Scaphoids	1	1	1	2	0.50	1.71	50.63
Lunates	0	0	0	2	0.00	0.00	50.63
Triquetrals	1	1	1	2	0.50	1.71	52.33
Pisiforms	0	0	0	2	0.00	0.00	52.33
Trapeziums	2	2	2	2	1.00	3.41	55.75
Trapezoids	2	2	2	2	1.00	3.41	59.16
Capitates	1	1	1	2	0.50	1.71	60.86
Hamates	1	1	1	2	0.50	1.71	62.57
Metacarpals	16	10	10	10	1.00	3.41	65.98
Hand phalanges	19	18	18	28	0.64	2.19	68.18
Femora	6	2	2	2	1.00	3.41	71.59
Patellae	0	0	0	2	0.00	0.00	71.59
Tibiae	4	2	2	2	1.00	3.41	75.00
Fibulae	5	2	2	2	1.00	3.41	78.42
Tali	2	2	2	2	1.00	3.41	81.83
Calcanei	2	2	2	2	1.00	3.41	85.24
Cuboids	1	1	1	2	0.50	1.71	86.95
Cuneiforms I	2	2	2	2	1.00	3.41	90.36
Cuneiforms II	1	1	1	2	0.50	1.71	92.07
Cuneiforms III	1	1	1	2	0.50	1.71	93.78
Naviculars	1	1	1	2	0.50	1.71	95.48
Metatarsals	15	10	10	10	1.00	3.41	98.89
Pedal phalanges	10	9	9	28	0.32	1.10	100.00

Abbreviations: NISP = Number of Identified Specimens, MNE = Minimum Number of Elements, MNAU = Minimum Number of Anatomical Units, Cumulative % MNAU = Cumulative percentage of the minimum number of anatomical units.

* The vertebrae and ribs are very fragmented. Here we indicate the NISP after all the possible refits were performed.
** Gómez-Olivencia, unpublished data.

SOM Table S2

Comparative sample of ear ossicles used in the present study.

Specimen/Group		Malleus	Incus	Stapes	Oval window	Source
Middle Pleistocene Europe						
	AT-84				X	Martínez et al., 2004
	AT-421				X	Martínez et al., 2004
	AT-667 (Cranium 5)			X	X	Martínez et al., 2004
	AT-3746+3747	X	X			Martínez et al., 2004
	Ehringsdorf H1026	X	X		X	Stoessel et al., 2016a
	Biache-Saint-Vaast 1	X	X			Lisoněk and Trinkaus, 2006; Crevecoeur, 2007
Neandertals						
	La Ferrassie 1	X	X	X		This study
	La Ferrassie 3	X	X	X	X	Quam et al., 2013b
	La Ferrassie 4 bis				X	Quam et al., 2013b
	La Ferrassie 5				X	Quam et al., 2013b
	La Ferrassie 8			X		Gómez-Olivencia et al., 2015
	Subalyuk 2			X		Quam et al., 2013b
	Amud 7		X			Quam and Rak, 2008
	Arcy-sur-Cure				X	Quam et al., 2013b
	Kebara 1				X	Quam et al., 2013b
	Neandertal sample	(n = 4)	(n = 10)	(n = 5)	(n = 13)	Stoessel et al., 2016a
Fossil *H. sapiens*						
	Qafzeh 3				X	Quam et al., 2013b
	Qafzeh 11	X	X		X	Quam and Rak, 2008; Quam et al., 2013b
	Qafzeh 12	X	X		X	Quam and Rak, 2008; Quam et al., 2013b
	Qafzeh 13				X	Quam et al., 2013b
	Qafzeh 15	X	X			Quam and Rak, 2008
	Qafzeh 21		X		X	Quam and Rak, 2008; Quam et al., 2013b
	Skhul 1				X	Quam et al., 2013b
	Border Cave 3				X	Quam et al., 2013b
	Nazlet Khater 2	X				Crevecoeur, 2007
	Pestera cu Oase 2	X		X		Ponce de León and Zollikofer, 2013
	Dolní Věstonice 14	X	X			Lisoněk and Trinkaus, 2006; Quam and Rak, 2008
	Dolní Věstonice 15		X			Lisoněk and Trinkaus, 2006; Quam and Rak, 2008
	Cro-Magnon 1	X	X	X		Stoessel et al., 2016a
	Cro-Magnon 2				X	Quam et al., 2013b
	Abri Pataud 1	X	X			Stoessel et al., 2016a
	Lagar Velho 1	X	X			Quam and Rak, 2008

	Parpalló 1				X	Quam et al., 2013b
Recent *H. sapiens*		(n = 43)	(n = 43)	(n = 40)		Quam and Rak, 2008; Quam et al., 2013b

SOM Table S3
Measurement protocol for the malleus.

No.	Definition	Description
	Orientation	Bone is lying on its posterior aspect (with the articular facet away from the observer) and with the manubrium parallel to the plane of projection, i.e., flat on the surface.
	X-axis (Head/neck axis)	Defined by a line connecting the midpoint of the minimum neck width and the most salient point along the top of the head. This is a slightly different definition than that of Masali (see text).
	Y-axis (Manubrium axis)	Defined by a line connecting the inferiormost points of the short process and the manubrium tip.
1	Total length	Maximum distance from the tip of the manubrium to the top of the head.
2	Manubrium length	Distance from the tip of the short process to the manubrium tip, following the Y-axis.
3	Manubrium M-L thickness	M-L thickness of the manubrium at mid-manubrium length, taken perpendicular to the Y-axis
4	Arc depth of the manubrium	Maximum depth of the curvature of the arc of the manubrium, measured from the point of maximum depth to the Y-axis.
5	Corpus length	Distance from the tip of the head to the lower border of the manubrium, taken following the X-axis.
6	S-I head width	Maximum distance between two parallel lines marking the widest points of the margin of the head, taken perpendicular to the X-axis.
7	Neck width	Minimum distance between the anterior and posterior borders of the neck.
8	Angle between the axes (M)	Angle formed between the X- and Y-axes.
	Manubrium/length index	(Manubrium length/total length)× 100
	Manubrium robusticity index	(Manubrium M-L thickness/manubrium length) × 100
	Manubrium/corpus index	(Manubrium length/corpus length) × 100
	Corpus/length index	(Corpus length/total length) × 100

SOM Table S4
Measurement protocol for the incus.

No.	Definition	Description
	Orientation	Bone is lying on its medial aspect. In this orientation, more of the articular facet is visible and the lowest point of the articular facet is marked by a 'lip'
	X-axis (Long process axis)	Defined by a line joining the tip of the long process to the most salient point along the superior border of the body.
	Y-axis (Short process axis)	Defined by a line joining the tip of the short process to the most salient point along the anterior portion of the superior border of the body.
	Z-axis (Rotational axis)	Defined by a line joining the tip of the short process to the most external point along the margin of the articular facet. This axis approximates the rotational axis of the incus within the tympanic cavity.
9	Short process length	Maximum distance from the tip of the short process to the most salient point along the anterior portion of the superior border of the body, following the Y-axis.
10	Long process length	Maximum distance from the tip of the long process to the most salient point along the superior border of the body.
11	Articular facet height	Maximum height of the articular facet taken perpendicular to the Z-axis.
12	Functional length	Maximum distance from the tip of the long process to the Z-axis, taken perpendicular to the Z-axis.
13	Arc depth of the long process	Maximum depth of the arc along the long process, measured from the plane defined by the lateralmost edge of the articular facet and the lateralmost point along the tip of the long process.
14	Inter-process length	Maximum distance between the most salient points along the superior margin of the short process and the tip of the long process. The lateralmost points of the short and long process tips define the measurement plane.
15	Inter-process arc depth	Maximum depth of the curvature between the short and long crurae tips. The depth is taken perpendicular to the axis defined above for the intercrural length (No. 14).
16	Angle between the axes	Angle formed between the X- and Y-axes.
	Crural index	(Short process length/long process length) × 100

SOM Table S5
Measurement protocol for the stapes.

No.	Definition	Description
	Bone orientation	Bone is lying flat on the surface with the convex (round) side turned toward the observer. This is the "norma craniale" orientation of Masali.
	X-axis (Anterior crus axis)	Defined by a line joining the antero-superior corner of the footplate and the tip of the head.
	Y-axis (Posterior crus axis)	Defined by a line joining the postero-superior corner of the footplate and the tip of the head.
	Z-axis (Footplate axis)	Defined by a line joining the most inferior points along the footplate margin anteriorly and posteriorly.
19	Total height of the Stapes	Maximum height from the lower margin of the footplate to the tip of the head, taken perpendicular to the Z-axis.
20	Head height	Minimum distance between the superior margin of the obturator foramen and the top of the head, taken perpendicular to the Z-axis. The latter point is defined as for total staps height (No. 19).
21	Obturator foramen height	Maximum height of the obturator foramen taken perpendicular to the Z-axis.
22	Obturator foramen width	Maximum width of the obturator foramen taken parallel to the Z-axis.
24	Posterior crus length	Maximum distance from the postero-superior corner of the footplate to the tip of the head, following the Y-axis.
26	Anterior crus length	Maximum distance from the antero-superior corner of the footplate to the tip of the head, following the X-axis.
28	Angle A	Angle between the anterior and posterior crurae, or between the X- and Y-axes.
29	Angle B	Angle between the anterior crus and the footplate, or between the X- and Z-axes.
30	Angle C	Angle between the posterior crus and the footplate, or between the Y- and Z-axes.
31	Footplate length	Maximum length of the footplate.
32	Footplate width	Maximum width of the footplate, not necessarily perpendicular to the length.
33	Footplate area	Measured area of the footplate.
	Stapedial index	(Footplate length/height of the stapes) × 100
	Obturator foramen index	(Obturator foramen width/obturator foramen height) × 100
	Foot plate index	(Footplate width/footplate length) × 100
	Crural index	(Anterior crus length/posterior crus length) × 100

SOM Table S6
Coding for the presence and degree of development of the pathological lesions of the surfaces and edges of both the vertebral body and articular facets[a].

Anatomical region	Code	Description
Subchondral bone (articular facets)	0	Normal
	1	Porosity
	2	Eburnation, destruction of the subchondral surface (porosity), or fusion
Osteophytic lipping (vertebral body and articular surfaces)	0	None
	1	Trace (<1 mm)
	2	Moderate (<4 mm)
	3	Major (>4 mm)
Intervertebral disc surfaces (vertebral bodies)	0	Good condition
	1	Porosity
	2	Schmorl's node, destruction of the subchondral surface (porosity), or eburnation.

[a]Following Dawson and Trinkaus (1997), modified from Bridges (1994).

SOM Table S7

La Ferrassie 1 vertebral pathology from the elements kept in Box 37.

	Anatomical position	C1	C2	C3	C4	C5	C6	C7	T1	T2	T3	T4?	T5-T11	T4?	T9?	T5-T8	T5-T8	T12
	Label*	#a	#b (2)	#d (3)	#c (4)	#e (5)	#f (6)	#g (7)	#h (8)	#i (9)	#j (10)	#k1	#k2	#k3 +#k 4+# k5	#p (13)	#m	#q	#r
Cranial facets	Right surface	0	0	0	0	0	0	0?	0?	0	X						0	X
	Right margin	0?	X	2	2	1	1	X	2	2	X						X	X
	Left surface	0	0	1	0	0	0	0	0	0	0		0				X	X
	Left margin	0?	1?	2	2	2	2	1	2	2	X		1				X	X
Caudal facets	Right surface	0	0	0	0	0	0	0	0	0	0						0	X
	Right margin	X	2	2	2	2	2	2	X	1	X						X	X
	Left surface	0	1	0	0	0	0	0	0	0	X			1	0		0	0
	Left margin	1	3	1	2	2	1	1	X	X	X			1	1		X	2?
Cranial body	Surface	-	-	0	0	0	0	X	X	0	X	0?				X	X	0?
	Ventral	-	-	1?	X	X	X	X	X	X	X	X				X	X	X
	Dorsal	-	-	0	0	X	0	X	X	X	0?	0				1	X	X
	Right	-	-	1?	X	X	X	X	X	X	X	X				X	X	X
	Left	-	-	1?	X	0	1?	X	X	X	X	X				X	X	0
Caudal body	Surface	-	0	0	0	0	0	0?	0	0	0?	0?				X	X	0?
	Ventral	-	X	X	0?	0?	X	X	X	1?	X	X				X	X	X
	Dorsal	-	1	0	1	1	1	1	1	1	1	0				2	1	1
	Right	-	1?	0	1	X	X	X	X	1?	1?	X				X	X	X
	Left	-	1?	0	1	X	X	X	X	1?	1?	X				X	X	0?
Costal facets (vertebral body)	Right surface								X	X	X	0				0	X	X
	Right margin								X	X	X	X				X	X	X
	Left surface								X	X	0	0				0	0	0
	Left margin								X	X	X	0				X	X	2
Costal facets (transverse process)	Right surface								X	0	0							-
	Right margin								X	X	X							-
	Left surface								X	X	X							-
	Left margin								X	X	X							-

*Following Gómez-Olivencia, 2013.

Subchondral bone: 0 = normal; 1 = porosity; 2 = eburnation, destruction of the subchondral surface (porosity), or fusion.

Osteophytic lipping: 0 = none; 1 = trace (<1 mm); 2 = moderate (<4 mm); 3 = major (>4 mm).

Intervertebral disc surfaces: 0 = good condition; 1 = porosity; 2 = Schmorl's node, destruction of the subchondral surface (porosity), or eburnation**.**

SOM Table S8

La Ferrassie 1 vertebral pathology from the elements kept in Box 38.

	Anatomical position	T7-T8?	T9	T	L1?	L3?	L2	L3	L4	L5
	Label	#z	#s1	#s2	#t2	#x	#aa (21)	#ab (22)	#ad (23)	#ac (24)
Cranial facets	Right surface		X	0					0	0?
	Right margin		X	1					1	X
	Left surface		X	X				0	0	0-1
	Left margin		X	X				X	1	2
Caudal facets	Right surface		X	X				0	0	0
	Right margin		X	X				1	1	1-2
	Left surface		X	X			0	0	0	0
	Left margin		X	X			2	3	3	2
Cranial body	Surface	0?	X	X	X	0-1				
	Ventral	X	X	X	2	2				
	Dorsal	1	X	X	X	0				
	Right	X	X	X	X	3				
	Left	X	X	X	X	X				
Caudal body	Surface	X	0?	X	0?	0				
	Ventral	X	X	X	X	X				
	Dorsal	2	0	X	0	0				
	Right	X	X	X	2	1				
	Left	X	X	X	X	1+				
Costal facets (vertebral body)	Right surface	X	0	X						
	Right margin	1	X	X						
	Left surface	X	0?	X						
	Left margin	X	0?	X						

Subchondral bone: 0 = normal; 1 = porosity; 2 = eburnation, destruction of the subchondral surface (porosity), or fusion.
Osteophytic lipping: 0 = none; 1 = trace (<1 mm); 2 = moderate (<4 mm); 3 = major (>4 mm).
Intervertebral disc surfaces: 0 = good condition; 1 = porosity; 2 = Schmorl's node, destruction of the subchondral surface (porosity), or eburnation.

SOM Table S9

Evidences of scoliosis in the LF1 spine.

Physical label	Virtual label[a]	Anatomical position	Vertebral body (larger side)[b] (Right/Left)	Articular pillar/mass (larger side) (Right/Left)	Spinous process twisting (in cranial view)	Rotation of the spinous process (in dorsal view)[c]
	#a	C1	X	-	X	X
2	#b	C2	-	R (Left pathologically remodelled)		
3	#d	C3	L (15.0/17.0)	R (Left pathologically remodelled) (8.5/6.4)	L (~7º)	Broken spinous process
4	#c	C4	-	R (13.5/11.0)	R (~8º)	
5	#e	C5	-	L (9.9/11.3)	Straight	No rotation
6	#f	C6	-	= (12.4/12.4)	Straight	No rotation
7	#g	C7	-	-	R (~8º)	
8	#h	T1	-	R ((30.2)/28.2)	R (~7º)	Clockwise (?). Tip missing.
9	#i	T2	R (17.3/16.5)	R (36.4/(34.0))	R (~5º)	Clockwise (~10º). Tip missing.
10	#j	T3	-	-	-	-
11	#k1	T4?	-			
11	#k3+#k4	T4?			R	Clockwise (?)
14	#q	T7			Straight?	No rotation (?)
19	#r	T12	= (23.7/24.0)	-	-	-
	#x	L3?	L (22.6/25.7)			
22	#ab	L3	-	L (based on the crcd larger lower left facet)	-	Clockwise (?)
23	#ad	L4	-	R (48.6/(48.0)) Left side pathologically remodelled	L (~3º)	-
24	#ac	L5	-	-	Straight?	Clockwise (~20-25º)

[a]Following Gómez-Olivencia, 2013.

[b]In cervical vertebrae, it refers to the development of the uncinate processes.

[c]No rotation refers to a rotation degree of <5º.

X=This anatomical region does not exist in this vertebra.

- = Not possible to assess, due to preservation.

In the cervical vertebrae, the thickness of the articular pillars has been measured from the inferior surface (positioning the caliper parallel to the orientation of the facet), to the middle of the upper facet.

In thoracic and lumbar vertebrae, we have measured the bi-articular diameter, i.e., from the cranialmost point of the upper articular facet to the caudalmost point of the inferior articular facet.

SOM Table S10

Absolute values[a] and percentage asymmetry[b] for the clavicular curvatures in cranial and dorsal views

Specimen	Species	Cranial view						Dorsal view					
		Internal curvature			External curvature			Inferior curvature			Superior curvature		
		R	L	% asym.	R	L	% asym.	R	L	% asym.	R	L	% asym.
La Ferrassie 1	*H. neanderthalensis*	13.2	12.3	7.3	14.2	17.7	24.6	5.4	8.2	51.8	5.8	2.6	123.1
Kebara 2	*H. neanderthalensis*	11.3	11.1	1.8	9.5	16.5	73.7	3.4	4.9	44.1	0.0	0.0	0.0
Regourdou 1	*H. neanderthalensis*	10.0	11.9	19.0	14.5	13.2	9.8	7.4	3.0	146.7	8.0	3.2	150.0
KNM-WT 15000	*Homo erectus*	13.1	15.3	16.8	14.6	14.7	0.7	5.0	5.3	6.0	7.4	8.1	9.5

R = Right; L = Left; asym. = asymmetry.

[a]Values from Voisin (2006).

[b]Calculated following Franciscus and Churchill, 2002.

References

Bridges, P.S., 1994. Vertebral arthritis and physical activities in the prehistoric Southeastern United States. Am. J. Phys. Anthropol. 93, 83–93.

Crevecoeur, I., 2007. New discovery of an Upper Paleolithic auditory ossicle: The right malleus of Nazlet Khater 2. J. Hum. Evol. 52, 341–345.

Dawson, J.E., Trinkaus, E., 1997. Vertebral osteoarthritis of the La Chapelle-aux-Saints 1 Neanderthal. J. Archaeol. Sci. 24, 1015–1021.

Franciscus, R.G., Churchill, S.E., 2002. The costal skeleton of Shanidar 3 and a reappraisal of Neandertal thoracic morphology. J. Hum. Evol. 42, 303–356.

Gómez-Olivencia, A., 2013. The presacral spine of the La Ferrassie 1 Neandertal: a revised inventory. Bull. Mém. Soc. Anthropol. Paris 25, 19–38.

Gómez-Olivencia, A., Crevecoeur, I., Balzeau, A., 2015. La Ferrassie 8 Neandertal child reloaded: New remains and re-assessment of the original collection. J. Hum. Evol. 82, 107–126.

Lisoněk, P., Trinkaus, E., 2006. The auditory ossicles. In: Trinkaus, E., Svoboda, J. (Eds.), Early Modern Human Evolution in Central Europe: The People of Dolní Věstonice and Pavlov. Oxford University Press, Oxford, pp. 153–155.

Martínez, I., Arsuaga, J.-L., Quam, R., Lorenzo, C., Gracia, A., Carretero, J.-M., Rosa, M., Jarabo, P., Carbonell, E., Bermúdez De Castro, J.-M., 2004. Auditory capacities in Middle Pleistocene humans from the Sierra de Atapuerca in Spain. Proc. Natl. Acad. Sci. USA 101, 9976–9981.

Ponce de León, M., Zollikofer, C.P.E., 2013. The internal cranial morphology of Oase 2. In: Trinkaus, E., Constantin, S., Zilhão, J. (Eds.), Life and Death at the Pestera cu Oase. A Setting for Modern Human Emergence in Europe, pp. 332–347.

Quam, R., Rak, Y., 2008. Auditory ossicles from southwest Asian Mousterian sites. J. Hum. Evol. 54, 414–433.

Quam, R., Martínez, I., Arsuaga, J.L., 2013. Reassessment of the La Ferrassie 3 Neandertal ossicular chain. J. Hum. Evol. 64, 250–262.

Stoessel, A., David, R., Gunz, P., Schmidt, T., Spoor, F., Hublin, J.-J., 2016a. Morphology and function of Neandertal and modern human ear ossicles. Proc. Natl. Acad. Sci. USA 113, 11489–11494.

Voisin, J.-L., 2006. Krapina and other neanderthal clavicles: a peculiar morphology? Period. Biol. 108, 331–339.